STARS

STARS

University of Central Florida
STARS

Electronic Theses and Dissertations, 2004-2019

2015

Response of Streamflow and Sediment Loading in the Apalachicola River, Florida to Climate and Land Use Land Cover Change

Paige Hovenga
University of Central Florida

Part of the Civil Engineering Commons

Find similar works at: https://stars.library.ucf.edu/etd

University of Central Florida Libraries http://library.ucf.edu

This Masters Thesis (Open Access) is brought to you for free and open access by STARS. It has been accepted for inclusion in Electronic Theses and Dissertations, 2004-2019 by an authorized administrator of STARS. For more information, please contact STARS@ucf.edu.

STARS Citation

Hovenga, Paige, "Response of Streamflow and Sediment Loading in the Apalachicola River, Florida to Climate and Land Use Land Cover Change" (2015). *Electronic Theses and Dissertations, 2004-2019*. 5171.
https://stars.library.ucf.edu/etd/5171

RESPONSE OF STREAMFLOW AND SEDIMENT LOADING IN THE APALACHICOLA
RIVER, FLORIDA TO CLIMATE AND LAND USE LAND COVER CHANGE

by

PAIGE ADELLE HOVENGA
B.S. University of Central Florida, 2013

A thesis submitted in partial fulfillment of the requirements
for the degree of Master of Science
in the Department of Civil, Environmental, and Construction Engineering
in the College of Engineering and Computer Science
at the University of Central Florida
Orlando, Florida

Fall Term
2015

Major Professor: Stephen C. Medeiros

ABSTRACT

Located in Florida's panhandle, the Apalachicola River is the southernmost reach of the Apalachicola-Chattahoochee-Flint (ACF) River basin. Streamflow and sediment drains to Apalachicola Bay in the Northern Gulf of Mexico, directly influencing the ecology of the region, in particular seagrass and oyster production. The objective of this study is to evaluate the response of runoff and sediment loading in the Apalachicola River under projected climate change scenarios and land use / land cover (LULC) change. A hydrologic model using the Soil Water Assessment Tool (SWAT) was developed for the Apalachicola region to simulate daily discharge and sediment load under present (circa 2000) and future conditions (circa 2100) to understand how the system responds over seasonal and event time frames to changes in climate, LULC, and coupled climate / LULC. These physically-based models incorporate a digital elevation model (DEM), LULC, soil maps, climate data, and management controls. Long Ashton Research Station-Weather Generator (LARS-WG) was used to create downscaled stochastic temperature and precipitation inputs from three Global Climate Models (GCM), each under Intergovernmental Panel on Climate Change (IPCC) carbon emission scenarios for A1B, A2, and B1. Projected 2100 LULC data provided by the United States Geological Survey (USGS) EROS Center was incorporated for each corresponding IPCC scenario. Results indicate climate change may induce seasonal shifts to both runoff and sediment loading, acting to extend periods of high flow and minimum sediment loadings or altering the time at which these events occur completely. Changes in LULC showed minimal effects on flow while more sediment loading was associated with increased agriculture and urban areas and decreased forested regions. A nonlinear response for both streamflow and sediment loading was observed by coupling climate and LULC change into the hydrologic model,

indicating changes in one may exacerbate or dampen the effects of the other. Peak discharge and sediment loading associated with extreme events showed both increases and decreases in the future, with variability dependent on the GCM used. Similar behavior was observed in the total discharge resulting from extreme events and increased total sediment load was frequently predicted for the A2 and A1B scenarios for simulations involving changes in climate only, LULC only, and both climate and LULC. Output from the individual GCMs predicted differing responses of streamflow and sediment loading to changes in climate on both the seasonal and event scale. Additional region-specific research is needed to better optimize the GCM ensemble and eliminate those that provide erroneous output. In addition, future assessment of the downscaling approach to capture extreme events is required. Findings from this study can be used to further understand climate and LULC implications to the Apalachicola Bay and surrounding region as well as similar fluvial estuaries while providing tools to better guide management and mitigation practices.

Dedicated to my loving mother, Julie Hovenga

ACKNOWLEDGMENTS

TABLE OF CONTENTS

LIST OF FIGURES

LIST OF TABLES

CHAPTER 1: INTRODUCTION

Climate change and the consequent long-term effects at both global and local scales have come to the forefront in the scientific, political, and public communities. Agreed by most scientists to be the main source of current global warming, natural and human drivers alter the level of greenhouse gases, e.g., water vapor, carbon dioxide, and methane, in the atmosphere which restrict or prevent the release of heat to space. Increased carbon dioxide concentrations are attributed largely to fossil fuel use and change in land use, while agriculture is principally credited with the increase in methane and nitrous oxide [*IPCC*, 2007]. Climate change is typically characterized by shifts in temperature and precipitation. Response is region specific and includes alteration of extremes, intensities, frequencies, spatial distributions, and temporal patterns [*Easterling et al.*, 2000; *Karl and Knight*, 1998; *Pal et al.*, 2013; *D Wang et al.*, 2013]. These changes impact the hydrologic cycle and have broad implications for fresh water resources in terms of both water quantity e.g., streamflow, and quality e.g., sediment and nutrient loading [*Milly et al.*, 2008; *D Wang and Hejazi*, 2011].

While climate change policies often focus on atmospheric composition, another major driving force is land use change, which can affect climate both regionally and globally by shifting physical properties and altering the surface-energy budget and carbon cycle [*Pielke et al.*, 2002]. Land coverage is altered progressively and abruptly as a result of socio-economic and biophysical drivers that are directed by human-environment conditions [*Lambin et al.*, 2001]. Biophysical drivers include alterations brought on by climate change, e.g., drought and sea level rise, further complicating the interaction between changes in climate and land use. Since land types differ in

physical and chemical properties, alterations as land classes expand, migrate, or change entirely can have an impactful influence on freshwater quantity and quality. Agricultural irrigation alone accounts for 85% of the total consumptive use and is linked to increased erosion, sediment load, and introduction of chemicals and nutrients while urbanization results in decreased groundwater recharge, increased runoff and sediment loading, sedimentation, and eutrophication [*Foley et al.*, 2005; *Gleick*, 2003; *Zimmerman et al.*, 2008].

As population increases, recent changes have shown urban population to be growing more rapidly, especially for developing countries [*Lambin et al.*, 2003]. The global population as of 2015 is estimated at 7.3 billion and is projected to reach 11.2 billion by the year 2100 [*United Nations et al.*, 2015]. Of that, an estimated 23% of the present global population live within 100 km of the coast and developments are expected to grow [*Small and Nicholls*, 2003]. Increased water demand and wastewater effluent associated with population growth and related land use changes has implications for the ecology and health of coastal habitats. While previous research into the effects of land use changes on hydrologic processes exists, many focus on historical land changes with interests typically isolated to water quantity or quality and those that do assess future conditions are often specialized and limited by the land class changes that are imposed, e.g., only urban development [*Asselman et al.*, 2003; *Johnson et al.*, 2012; *Schilling et al.*, 2010; *Schilling et al.*, 2008b; *Shi et al.*, 2007; *Ward et al.*, 2009]

The objective of this research is to assess the impacts of projected climate and land use land cover (LULC) change on streamflow and sediment loading, both seasonal and event scale, in the Apalachicola River, Florida. To do so, a hydrologic model using the Soil Water Assessment Tool

(SWAT) was developed for the Apalachicola region to simulate daily discharge and sediment load under present (circa 2000) and future conditions (circa 2100).

The physically-based SWAT model incorporates a digital elevation model (DEM), LULC, soil maps, climate data, and management controls. Long Ashton Research Station-Weather Generator (LARS-WG) was used to create downscaled stochastic temperature and precipitation inputs from three Global Climate Models (GCM), each under Intergovernmental Panel on Climate Change (IPCC) carbon emission scenarios A1B, A2, and B1. These scenarios represent potential future emissions resulting from a range driving forces, e.g. social, economic, environmental, and technologic. Projected 2100 LULC data provided by the United States Geological Survey (USGS) Earth Resources Observation and Science (EROS) Center was incorporated for each corresponding IPCC scenario. Streamflow and sediment loading response to changes in climate, LULC, and coupled climate / LULC was evaluated.

This research is significant in that many species of this region, in particular seagrass and oyster beds, are sensitive to salinity and total suspended solids levels which can affect productivity and spatial distributions. Streamflow and sediment from the Apalachicola River drain to Apalachicola Bay in the Northern Gulf of Mexico, and alterations resulting from climate change, e.g., changes in temperature and rainfall extremes intensities, frequencies, spatial distributions, and/or LULC change, e.g., changes in physical and chemical surface properties, will have in a direct influence on the ecology of the region by changing processes related to the hydrologic cycle including runoff, groundwater recharge, evapotranspiration, and sediment, nutrient and chemical loading. Results from this study can be used to further understand climate and LULC implications to the

Apalachicola Bay and surrounding region as well as similar fluvial estuaries, while provide tools to better guide management and mitigation practices, and aid in future hydrologic assessments of climate and LULC change.

CHAPTER 2: LITERATURE REVIEW

2.1 Historic Climate Change

The Intergovernmental Panel on Climate Change (IPCC), established in 1988 by the United Nations Programme (UNEP) and the World Meteorological Organization (WMO), is a collaborative body that reviews and assesses scientific findings related to climate change. The organization is divided into three Working Groups, a Task Force, and a Task Group. Working Groups I, II, and III respectively focus on the physical science of climate change, impacts and vulnerability of socio-economic and natural systems, and mitigation strategies. The joint effort of the working groups has resulted in a series of comprehensive reports that detail technical and scientific discoveries related to climate change for both the past, present, and future.

The IPCC Fourth Assessment Report (AR4) Working Group I Report: The Physical Science Basis provides a detailed account of the observed changes in climate, including those related to the atmosphere, surface, ocean, and cryosphere [*IPCC*, 2007]. A prevalent theme is the alteration of global temperatures. While the surface, ocean, and troposphere have shown an ever increasing warming trend, the stratosphere that provides the protective ozone layer has experienced cooling. Thermal expansion of the oceans and decreased snow and ice extents coincide with increases in temperature. Precipitation has also been altered globally, though the ways in which it has changed is region specific. In eastern parts of North America, rainfall has significantly increased and it is likely the frequency of heavy rainfall events will increase.

2.2 Modeling Climate Change Climate Models

Global Circulation Models (GCM), synonymously used with Global Climate Models, simulate climate by representing physical processes in the atmosphere, ocean, cryosphere and land surface within a three dimensional grid. To capture the global exchanges, the resolution is often quite coarse. Typical resolution is between 250 – 600 kilometers in the horizontal direction, 10 to 20 atmospheric vertical layers, and up to 30 ocean layers [*IPCC*, 2013]. Models usually provide monthly, 20 year, and 30 year means. Despite applying the same boundary conditions, the varying structures of GCMs including the spatial resolutions, individual physical process models, and interacting feedback loops can result in differing outputs between GCMs. Regardless of these differences, outputs typically agree on broad global warming.

In addition to an assessment of the historically observed climate change, the IPCC AR4 evaluates future projected climate changes resulting from both natural variability and human activity and their short and long term implications. The projections used were developed from a combined modeling effort of 18 groups worldwide, who performed a suite of simulations using GCM under various sets of driving scenarios [*IPCC*, 2007]. Driving forces reference possible future social, economic, environmental, and technological directions that alter carbon emissions as outlined in the Special Report Emission Scenarios (SRES) [*IPCC*, 2000]. IPCC-SRES, frequently referred to as carbon emission scenarios, are classified by four families, A1, A2, B1, and B2. Generally speaking, the A1 scenario describes a rapidly changing world with population increasing to 2050 and then decreasing by 2100. A1 is broken down further into groups A1B, A1FI, A1T that represent various ways in which technological change might be driven. A2 describes a more heterogeneous world with large gaps between economic and technologic constructs. B1 represents

a convergent world with the same population dynamics as those described by the A1 scenario and economic, social, and environmental choices are driven by global sustainability and conservation. B2 describes an increasing population at a rate slower than A2 and while development is geared toward sustainability, decisions are focused on more local and regional scale goals. While the scenarios may represent stark differences in future, global conditions, no one scenario is held to be more relevant than the other and all are viewed as equally probable outcomes.

2.3 Downscaling Techniques

While GCMs typically converge on global climate predictions, the coarse spatial and temporal resolutions typical of GCMs struggle to capture small scale processes occurring at regional or local scales [*Semenov and Stratonovitch*, 2010]. Several downscaling approaches, e.g., statistical, dynamic using regional climate models, and weather generators, have been developed to alleviate this dilemma. The statistical downscaling approach is performed by creating relationships, e.g., regressions or neural networks, that link large-scale climate "predictor" variables to regional or local variables or "predictands" [*Wilby et al.*, 2004]. This technique produces relatively quick results and is computationally inexpensive, however a major disadvantage is the assumed constant empirical relationships [*Mearns et al.*, 2004]. The issue of non-stationarity may be resolved using a stochastic approach [*Richardson*, 1981; *Wilby*, 1997]. Dynamic downscaling using regional climate models (RCMs) uses a nested high-resolution grid that is driven by boundary conditions derived from GCM. While RCMs typically model spatial patterns, precipitation extremes, and variability of daily and monthly values better than GCMs, the downscaling technique is computationally expensive and therefore few scenarios are usually derived [*Mearns et al.*, 2004]. In an assessment of statistical and dynamical RCM methods for 976 stations in Europe, *Murphy*

20

[1999] found that while the skill levels were comparable, statistical methods performed better for summer temperatures and downscaling via RCM was superior for winter rainfall. Stochastic weather generator (WG) algorithms develop climate change scenarios by adjusting present day parameters by monthly statistics derived from sampling distributions of the sums or averages of the daily values [*Richardson*, 1981; *Wilks*, 1992]. WGs are able to produce daily time series of indefinite lengths and capture changes in both climatic means and variability [*Wilks*, 1992]. WGs have been used in a number of studies to develop and asses climate change scenarios [*Favis-Mortlock and Boardman*, 1995; *Katz*, 1996; *Semenov and Barrow*, 1997; *Valdes et al.*, 1994; *Wilks*, 1992]

2.4 Mapping Land Use Land Cover

Artificial satellites have been used for decades to collect information about the earth. While an estimated 6,600 satellites have been launched into orbit, only near 1000 are operational [*ESA*, 2013]. Satellites equipped with data collecting instruments are able to capture images of earth at various regions of the electromagnetic scale. These data are used by scientists and engineers to assess and monitor land cover changes, urban sprawl, natural resources, toxic waste dumping, phytoplankton blooms, and flood inundation extent [*Binding et al.*, 2012; *Chaouch et al.*, 2012; *Taillant and Picolotti*, 1999].

In satellite imagery, a band constitutes a specific region of the electromagnetic spectrum, typically with respect to wavelength. Since materials reflect and absorb energy differently at various wavelengths, processing techniques can be used to extract or magnify signature traits of materials, making them easier to differentiate from one another. Techniques include visual interpretation,

vegetative indices, supervised classification, unsupervised classification, and band ratio-ing. For these reasons satellite imagery is used to identify, map, and evaluate historical change in land cover types and distributions.

2.5 Historical LULC Change

Efforts to quantify historical population and land use patterns over the past 300 years have led to the development of HYDE, the History Database of the Global Environment. An analysis of HYDE data by *Klein Goldewijk* [2001] suggests that from 1700 – 1990, global cropland and pasture have increased from 265 – 1471 and 524 – 3451 mega hectares (Mha), respectively, while forest / woodland loss is estimated at nearly 24%. In the United States, agriculture and pasture have increased 70-fold and 100-fold, respectively. Improved irrigation systems have resulted in the loss of numerous wetlands, especially within the Midwest and semi-arid regions.

To understand Earth's physical, biological, and chemical processes and their interactions with human influence on both regional and global scales, collaborative research efforts have been launched, including the International Geosphere-Biosphere Program (IGBP). A core research project of IGBP is Past Global Changes (PAGES) (http://www.pages-igbp.org/). Focus 4 of PAGES studies human-climate-ecosystem interactions to understand past states and better predict future conditions. One project of PAGES, the Land Use and Cover project, aimed to recreate past land cover maps from fossil pollen records and has since been replaced by LandCover6k. Building on the Land Use and Cover initiative, the project addresses climate induced, natural, and human induced land changes resulting from anthropogenic use. Outputs from this program will be improved HYDE and Kaplan and Krumhardt (KK), used to estimate anthropogenic deforestation

in Europe, models as well as reconstructed LULC for the Holocene periods [*Kaplan et al.*, 2009; *Klein Goldewijk*, 2001].

With particular focus on the United States, the USGS Land Cover Trends project was developed to understand patterns, rates, trends, causes, and consequences of LULC change. Initiatives set by the USGS Land Cover Trends resulted in modeled land use changes from 1973 - 2000 for the conterminous U.S. Change rates were developed for 84 ecoregions using Landsat imagery and a statistical sampling approach [*Loveland et al.*, 2002]. The Land Cover Trends project ran from 1999 through 2011. Research has since been continued by the Land Change Research Project.

In the Apalachicola region, *Pan et al.* [2013] used satellite imagery from Landsat Thematic Mapper (TM) to identify changes in land class from 1985 to 2005. From 1985 – 2005 the growth rate of urban areas was 79% and was typically convert from forest / woody wetland. From 1985 – 1996 shrub and barren land decreased. Forest / woody wetland also increased during this period before declining from 1996 - 2005 as a result of increased cropland / pasture from 1996 – 2005.

2.6 Modeling Future Land Use Land Cover Change

The effect land use changes have on the surface-energy budget and carbon cycle make accurate representation of historical and projected changes an important input for regional and global climate models. LULC change is fueled by biophysical (e.g., slope, soil properties, altitude) and socio-economic drivers (e.g., social, political, and economic factors) [*Lambin et al.*, 2003]. While data on the former is easier to quantify and more accessible, the latter can be more difficult to capture. Often correlated rather than causal metrics serve as a proxy to project changes e.g.,

population density used to estimate the allocation of cropland [*Klein Goldewijk*, 2001]. The detail of interaction between drivers is dependent on the spatial and temporal scales at which it is being modeled. Intricate relationships seen at the local scale become more difficult to identify at increasing extents. When modeling land changes, two points must be addressed, with the first often being easier to assess: 1) where do the changes take place and 2) what are the rates in which these changes progress [*Veldkamp and Lambin*, 2001]. Lastly, since biophysical processes are both affected and effect land use change, built in biophysical feedback loops are important to capture the dynamic interaction.

A well-known model used for projecting land cover is the FORecasting SCEnarios of Land-use Change (FORE-SCE). Originally developed to model regional land cover change in the Western Great Plains, FORE-SCE uses data from the Land Cover Trends project and theoretical, statistical, and deterministic modeling techniques to project future land cover [*T L Sohl et al.*, 2007]. The model incorporates various modules to address different characteristics of change, i.e., non-spatial proportions of land use change are provided by the DEMAND module and physical distributions are provided by a spatial allocation module. Since its original version, FORE-SCE has been adapted to include forest cutting and resultant changes in forest type and age [*T Sohl and Sayler*, 2008]

FORE-SCE has been used by researchers at the USGS Earth Resources Observation and Science (EROS) to create spatially and thematically detailed annual LULC maps for 2006 – 2100 [*USGS*, 2014a]. The maps were developed by implementing historic data from the Land Cover Trends project and information considering downscaled economic and environmental policies and

regional vs. global development that align with IPCC-SRES (Figure 1). Historical and future scenario maps contain 17 LULC classes and are available to the public to download in raster format (250 meter pixel resolution) for the conterminous U.S. (http://landcover-modeling.cr.usgs.gov/projects.php).
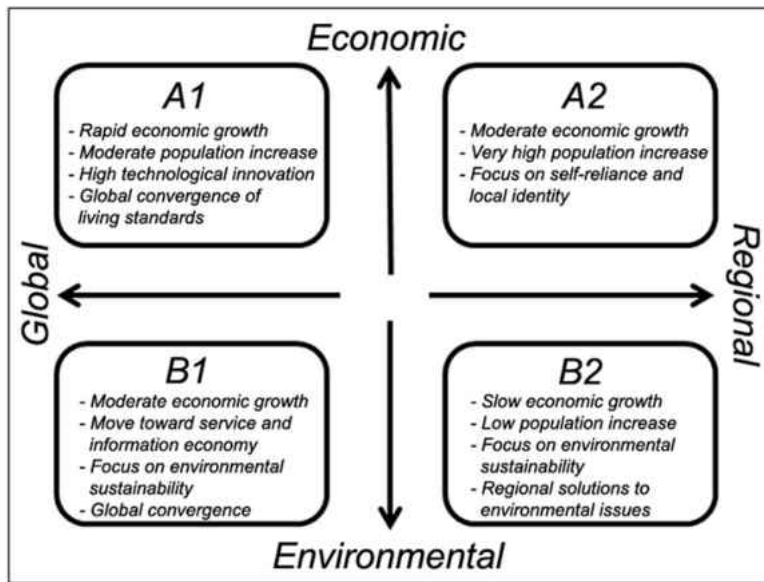
IPCC SRES storylines are oriented along two axes: 1) economic vs. environmental priorities, and 2) global vs. regional development. The four scenarios each describe divergent, yet plausible futures.

Figure 1 Adaptation of International Panel on Climate Change (IPCC) Special Report on Emission Scenarios (SRES) for projected LULC change [*USGS*, 2014b].

2.7 Climate / LULC Change and Hydrologic Modeling

This study focuses on impacts of climate and land use change on water quantity and quality in the southeastern United States, particularly the Apalachicola River Basin using the hydrologic model Soil and Water Assessment Tool (SWAT). Many studies have incorporated climate projections from regional climate models (RCMs) or downscaled global climate models into SWAT for this purpose [*Narsimlu et al.*, 2013; *Phan et al.*, 2011; *Shrestha et al.*, 2013]. Additionally, research

has assimilated land use change only and the coupling of climate and land use change into SWAT [*J Chen et al.*, 2005; *Park et al.*, 2011; *Schilling et al.*, 2008a; *Semadeni-Davies et al.*, 2008; *Yan et al.*, 2013]. Dependent on the study, climate vs. land use change impacts have been found to be more significant than the other and changes in one may amplify the effects of the other [*Praskievicz and Chang*, 2009].

Previous studies of climate and land use change that assess streamflow and sediment loading exist for the Apalachicola region. *X Chen et al.* [2014] evaluated both seasonal and event scale response of runoff and sediment loads using climatic data from two RCMs (HRM3-HADCM3 and RCM3-GFDL) using the Soil and Water Assessment Tool (SWAT). Seasonal response was determined to be only slight with contrasting behavior produced from the individual models. At the event scale, peak flow increased from the baseline by 8% for HRM3-HADCM3 and 50% for RCM3-GFDL. Peak sediment load increase was negligible for HRM3-HADCM3 and 89% for RCM3-GFDL. *Johnson et al.* [2012] used SWAT to investigate the sensitivity of streamflow and water quality to climate change and urban / residential development. Sensitivity of flow (both average and extreme) and sediment loading differed in response to climate change among the climate models and downscaling approaches used. While climate induced both increases and decreases in flow, the sediment was increased overall. Climate was also determined to be more impactful than land development at the large scale simulation. *Gibson et al.* [2005] focused on changes in flow regime (magnitude, duration, frequency, timing, and rate of change) under downscaled GCM change and projected human demand. Decreased flow variability and lower high and low flows were reported. *Hay et al.* [2014] studied the accuracy of downscaled climate data from three GCMs using an asynchronous regional regression model (ARRM), to simulate historical

conditions of streamflow using the Precipitation-Runoff Modeling System (PRMS). Based on the model skill evaluation, results indicated streamflow may be best evaluated at weekly or longer time steps. Additionally, model outputs can be significantly biased, and therefore relative change from historical conditions might be better suited to evaluate future conditions.

2.8 Ecologic and Hydrologic Studies

Many species found in the Apalachicola Estuary are affected by the alteration of streamflow and sediment loading. *H Wang et al.* [2008] coupled an oyster population model and hydrodynamic model to assess the response of oyster growth rates in Apalachicola Bay to changes in freshwater inflow. Growth rates, significantly correlated to salinity levels, were lowest during mid spring in times of high freshwater flow and consequent low salinity in the Bay while higher growth rates occurred during the summer when temperatures were warm and food supply was high. *Dekshenieks et al.* [2000] also found increased oyster larval growth rate associated with lower freshwater inflow and higher salinity while high levels of total suspended solids caused increased mortalities of oysters in larval development and decrease oyster filtration rates. *R.J. Livingston et al.* [2000] linked a hydrodynamic circulation model and oyster population dynamics for the Apalachicola Estuary and reported increased oyster mortality associated with high salinity, low-velocity current patterns, and proximity of oyster bars to high saline water from the Gulf. Findings by *Dutterer et al.* [2012] suggest flow regimes occurring in spring and summer that reduced the frequency and duration of floodplain inundation may reduce stream fish recruitment in the Apalachicola River. Seagrass growth, abundance, and morphology has been shown to be affected by nutrient-carrying sediment [*Short*, 1987]. Field / experimental and lab studies by *Robert J. Livingston et al.* [1998] of water quality, qualitative and quantitative light factors and sediment

characteristics indicate the distribution of submerged aquatic vegetation in the Northern Gulf of Mexico is controlled by salinity, temperature, depth, light attenuation, and sediment and nutrient supply. Alteration of seasonal patterns, extremes, and/or frequencies of both riverine freshwater inflow and sediment loading to the Apalachicola Bay has implications for shifting the ecology of the system.

The research developed herein comprehensively assesses the isolated and coupled impacts of climate and land use land cover change in the Apalachicola River region. Located in Florida's panhandle, the streamflow and sediment from the Apalachicola River drains to Apalachicola Bay within the Northern Gulf of Mexico, resulting in a direct influence on the ecology of the region, in particular seagrass and oyster production. Response to changes are evaluated at the seasonal and event scale. Downscaled climate data for three GCMs and LULC maps, detailing changes for sixteen distinct land classes, are both characterized by the IPCC-SRES A2, A1B, and B1 circa 2100. Previous studies for Apalachicola have limited climate change to one carbon emission scenarios and have focused singularly on anthropogenic changes in land use / land cover. In using IPCC-SRES correlated data, the forcing factors that drive climate change align with those that drive land use and cover change, providing a congruent foundation from which inter-comparisons can be made.

CHAPTER 3: DESCRIPTION OF STUDY DOMAIN

Located in the southeastern United States, the Apalachicola-Chattahoochee-Flint (ACF) River Basin extends to north Georgia, includes southeast Alabama, and covers part of Florida's Panhandle. Shown Figure 2 by the yellow boundary, the entire region covers a drainage area of approximately 51,282 km^2 (19,800 mi^2)[*U.S.G.S.*, 2014]. The Flint and Chattahoochee Rivers converge at Lake Seminole near the Florida-Georgia state line. The Jim Woodruff Lock and Dam marks the beginning of the Apalachicola River, a meandering river with extensive floodplains. Flowing to the south, it ultimately drains to Apalachicola Bay in the Northern Gulf of Mexico.

The Apalachicola Bay system is a shallow estuary divided into 4 sections, shown in Figure 3. Having a combined area of 44,608 hectares (110,228 acres), the average depths of East Bay, St. Vincent Sound, Apalachicola Bay, and St. George Sound are 0.7, 1.0, 2.1, 2.5 meters (2.3, 3.3, 6.9, and 8.2 feet), respectively [Huang and Jones, 1997]. The Bay is bounded by three offshore barrier islands: St. Vincent, St. George, and Dog Islands. The series of passes between the islands from east to west are East Pass, Sikes' Cut, West Pass, and Indian Pass. These passes allow the exchange of fresh and salt water, sediment, and nutrients between the Bay and Gulf.

Figure 2 Apalachicola-Chattahoochee-Flint River Basin in yellow and study domain in white.
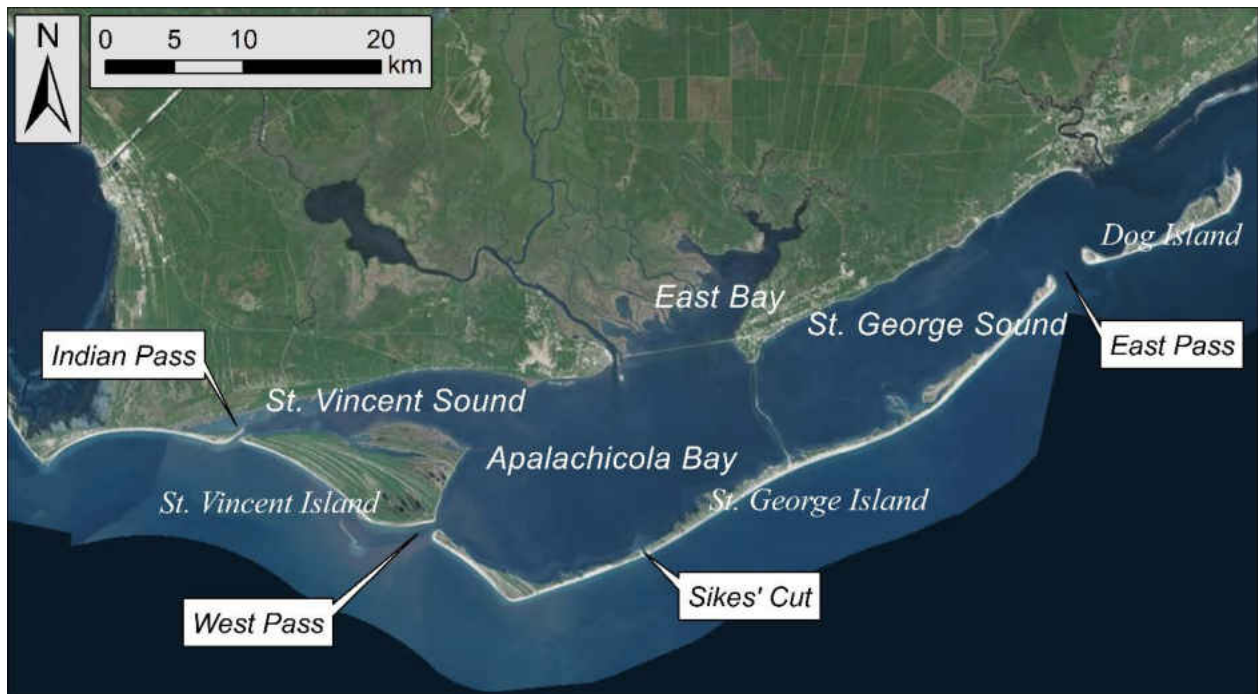
Figure 3 Apalachicola Bay system

This study focuses on the southern portion of the ACF River basin. The domain, indicated in white in Figure 2 and in more detail in Figure 4, includes the Apalachicola River, beginning in the north at the Jim Woodruff Lock and Dam near Chattahoochee, FL and extends south to the Apalachicola Bay. The tributary to the west, the Chipola River, is also included and stretches to the north as far as Dothan, Alabama. The Chipola River contributes 11% of Apalachicola River's total flow [*Elder et al.*, 1988]. The entire watershed study area is 575,930 hectares (1,423,154 acres) and is divided into a total of 99 subbasins. Elevation ranges from around 0 to 110 meters (0 to 361 feet), (NAVD88). Developed regions included in the domain, aside from Chattahoochee and Dothan, are Marianna, Bristol, Wewahitchka, Sumatra, Port St. Joe, and Apalachicola, Florida (Figure 4).
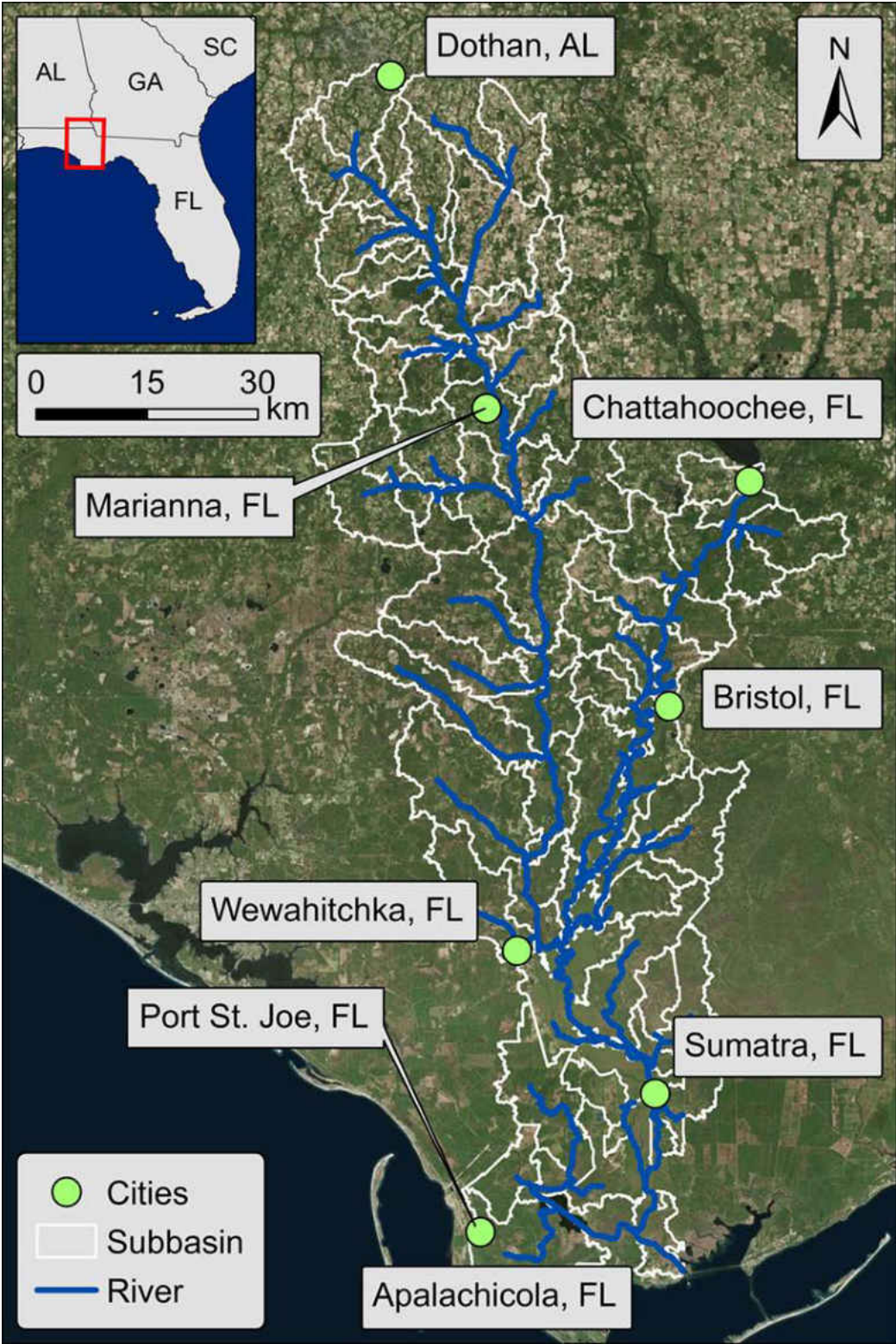
Figure 4 Study domain extending from Dothan, Alabama to Apalachicola Bay.

The Apalachicola River basin has a subtropical, humid climate, with mean annual temperature around 20° C (68° F) [*R.J. Livingston*, 1984]. Within the ACF, low temperatures in January vary from 4° - 13° C (39° - 55° F) and high temperatures vary from 24° - 27° C (75° - 81° F) in July [*Couch et al.*, 1996]. Average annual rainfall is approximately 150 centimeters (59 inches), though there is an uneven distribution with regions to the west of the river receiving one-third less rainfall that those to the east [*R.J. Livingston*, 1984]. Further, rainfall amount increases moving from the upstream (Chattahoochee) to midstream (Blountstown) and finally to downstream (Apalachicola) with an average annual rainfall of 116, 129, and 137 centimeters (46, 51, and 54 inches), respectively [*D Wang et al.*, 2013]. Seasonally there are two peaks, one in March and another occurring in late summer / early fall from July to September. Thunderstorms are frequent in Florida's Panhandle, occurring around 70 days out of the year, typically during the warm season around the afternoon and early evening [*Fuelberg and Bigger*, 1994].

The Apalachicola river has the largest discharge of all rivers in Florida and is ranked 21st in magnitude within the conterminous United States. It accounts for 35% of the freshwater inflow on the western coast of Florida [*McNulty et al.*, 1972]. Measured at Sumatra, Florida the average annual discharge from 1978 to 2012 was 24,000 cubic feet per second (680 cubic meters per second) with fluctuations ranging from 10,000 to 37,000 cubic feet per second (283 – 1048 cubic meters per second) [*USGS*, 2012]. The river experiences large seasonal fluctuations in flow, with peaks occurring January through April and lower flows experienced September through November [*R.J. Livingston*, 1984]. Tidal influences from the Bay do not extend upstream more than 25 miles or 40 kilometers [*Couch et al.*, 1996].

The Apalachicola River floodplain has three major types of soils: silt-clays (approximately 90%), sandy soils (approximately 8%), and organic soils (approximately 3%). Sandy soils are typically found on levees where high flows occur, greater than 80,000 cubic feet per second or 2,265cubic meters per second, and organic soils are more commonly found in swamp areas in the northern reach [*Light et al.*, 1996]. Sediment that does not settle out is ultimately discharged into Apalachicola Bay. The deposition rates for the Apalachicola system are greater than other estuaries in the Gulf Coast with relatively high sand content and low silt content. Samples from 1825 to 1900 indicate that historically silt was more prevalent in this system and while the quantity of sediment delivered to the Bay has remain unchanged since the 1950s, it is suggested that the abrupt changes in the sediment regime may have been caused by anthropogenic factors such as the implementation of dams [*Isphording*, 1986]. Once within the Bay, fine sediments are carried out to the Gulf of Mexico while sand is moved within the Bay by tidal currents [*R.J. Livingston*, 1984].

Significant to both the ecology and economy, the coastal estuarine system provides a habitat for many types of flora and fauna including salt marshes, seagrasses, and oyster beds, many of which are threatened or endangered. Salt marshes and seagrasses provide shelter and reproductive grounds for many terrestrial and aquatic species. Oysters beds are highly productive in this region and provide over 90% of Florida's and 8-10% of the nation's oysters [*R.J. Livingston*, 1984]. Many of these species are sensitive to salinity and total suspended solids which affect both their productivity and spatial distribution [*R.J. Livingston*, 1984; *Scavia et al.*, 2002]. Additionally, changes to flow and sediment can affect channel connectivity and alter floodplain extents, making the riverine influx an important component of the system [*Gibson et al.*, 2005]. Previous studies have found changes in climate and land use / land cover may affect both streamflow and sediment

loading by altering peaks and total quantities associated with extreme events, result in increases and decreases at the seasonal scale, shift flow variability, and that changes in one may amplify the effects of the other [*X Chen et al.*, 2014; *Gibson et al.*, 2005; *Johnson et al.*, 2012; *Praskievicz and Chang*, 2009]. Seasonal shifts have implications for threatening the phenology of the system, affecting migration, breeding, and distributions. As urban areas are expected to increase in coastal regions, sediment loading may also be increased, offsetting the sensitive balance at which seagrasses and oyster bed survive. Lastly, changes in extreme events may affect flooding and erosion rates. To better adapt to and mitigate adverse effects of climate and LULC change for this region, a comprehensive assessment and understanding of the response of streamflow and sediment to said changes is required.

CHAPTER 4: MODELING APPROACH

4.1 Simulation and Modeling Structure

From henceforth, the terms "present" will refer to circa 2000 and "future" will refer to circa 2100. The simulations can be broken into four distinct categories that are characterized by the climate and LULC data used: 1) baseline, 2) climate only, 3) LULC only and 4) climate and LULC (Table 1). The baseline incorporates present day climate and LULC. Climate only incorporates future climate and present land cover. LULC only implements present climate and future LULC. Climate and LULC uses both future climate and LULC.

Table 1 Dataset applied for simulation categories

	Baseline	**Climate Only**	**LULC Only**	**Climate & LULC**
Climate	Present	Future	Present	Future
LULC	Present	Present	Future	Future

Future climate is characterized by three IPCC carbon emission scenarios: A2, A1B, and B1. Climatic data for each scenario is predicted by three global climate models (GCMs): HadCM3 (HADCM3), IPSL-CM4 (IPCM4), and ECHAM5-OM (MPEH5). Therefore, when referring to climate change, a total of nine datasets are evaluated. Future LULC is also characterized by the three carbon emission scenarios, A2, A1B, and B1. LULC projections for individual GCMs do not exist and are therefore not assessed. Thus, when referring to LULC change, there are a total of three datasets that are evaluated. Further detail on the climate and LULC change datasets are discussed in subsequent chapters. When climate and LULC changes are both implemented in the

36

model, the datasets are matched according to the carbon scenarios, that is, A2 climate will be paired with A2 LULC. Therefore, when assessing the climate and LULC change simulations, there are a total of nine.

The modeling structure used has two main components which consist of the Long Ashton Research Station-Weather Generator (LARS-WG), used to downscale and prepare climate data and the Soil and Water Assessment Tool (SWAT), which was used to simulate hydrologic processes (Figure 5). Climate data created by LARS- WG serves as an input to the SWAT model.

4.2 Model Development

A hydrologic model using SWAT was developed for historical conditions (1984 – 1994) for the purpose of calibration and validation. This is represented by the box labeled "SWAT MODEL" in Figure 5. Inputs reflect the historical time period and include LULC, a digital elevation model (DEM), soil maps, weather, and boundary conditions. Datasets are described further in Chapter 5. The model performance was assessed via calibration and validation for the historical period. Once completed, the SWAT model was used to run all simulations under present and future conditions.

4.3 Present Conditions

To appropriately compare future with present conditions, climate data for both were prepared in an analogous way. The present day climate data used by SWAT was prepared by inputting observed weather from 1970 – 1999 into the Long Ashton Research Station-Weather Generator (LARS-WG). This is represented in Figure 5 by the box labeled "LARS- WG". The output was

30 years of stochastically developed weather data representative of present conditions, referred to as the "baseline". The present LULC data used by SWAT refers to the same dataset used in the model development, referencing 1992.

4.4 Future Conditions

To create future climate data, the same observed weather from 1970 – 1999 was input into the LARS- WG along with a scenario file, which includes the changes in climate parameters from 2000 to 2100. The changes refer to carbon emission scenarios, A2, A1B, and B1, as predicted by the three different GCMs. One scenario file exists for each carbon emission scenario and GCM, for a total of nine. The development of the scenario files is described in Chapter 6. Each scenario file was used by the LARS- WG to perturb the observed weather data and the output was 30 years of stochastically developed weather data, referred to as "future", and representative of future conditions. The future LULC data used by SWAT refers to the three carbon emission scenarios and is indicated by the box labeled 2100 LULC.

The climate and LULC data were incorporated into SWAT and outputs consisted of daily streamflow (cms) and daily, total sediment loading (tonnes/day), measured at single location near the watershed outlet. In the case where climate change was included in the simulation, a total of nine sets (each containing streamflow and sediment) were produced.   When LULC change was included in the simulation, a total of three sets (each containing streamflow and sediment) were produced and when climate and LULC was included in the simulation, a total of nine sets (each containing streamflow and sediment) were produced.
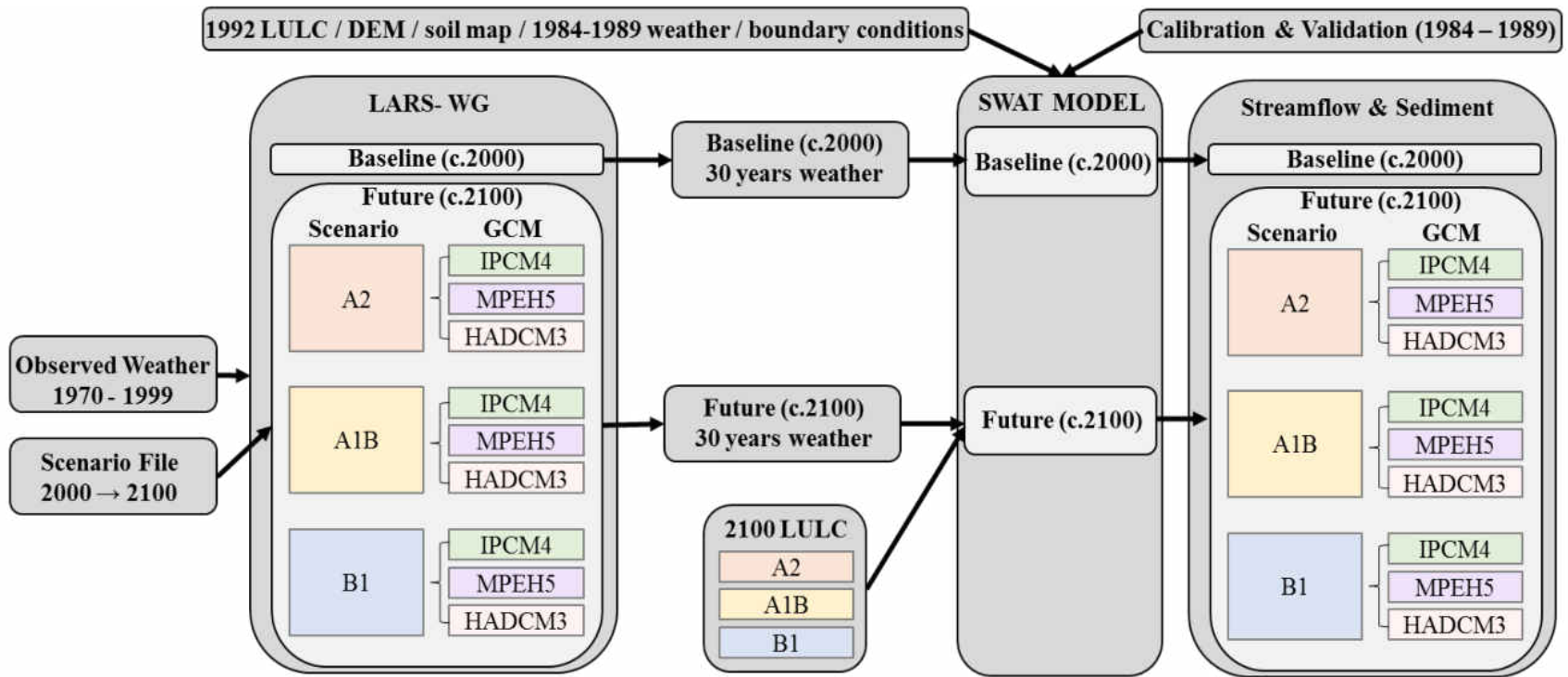
Figure 5 Modeling structure.

CHAPTER 5: HYDROLOGIC MODEL DEVELOPMENT

5.1 Model Description

The hydrological model selected for this study was the Soil and Water Assessment Tool (SWAT), a physically based, continuous time model that is designed to simulate long-term hydrologic processes within large watersheds [*Neitsch et al.*, 2011; *Srinivasan and Arnold*, 1994]. SWAT is an open source model capable of simulating both water quantity and quality on monthly and daily time scales. Surface runoff is simulated using the Soil Conservation Service (SCS) curve number method:

$$Q_S = \frac{(R_{day} - 0.2S)^2}{R_{day} + 0.8S} \qquad (1)$$

where Q_S is the accumulated surface runoff (mm), R_{day} is the rainfall depth (mm), and S is the retention parameter (mm) defined by:

$$S = 25.4 \left(\frac{1000}{CN} - 10 \right) \qquad (2)$$

where CN is the curve number [*SCS*, 1972]. The curve number is an empirical parameter based on land cover and soil type used to estimate runoff generated from rainfall. Sediment yield is related to the surface runoff and is computed from the Modified Universal Soil Loss Equation (MUSLE):

$$sed = 11.8 * \left(Q_s * q_{peak} * area_{hru} \right)^{0.56} * K_{USLE} * C_{USLE} * P_{USLE} * LS_{USLE} * CFRG \quad (3)$$

where sed is the sediment yield (tonnes/day), q_{peak} is the peak runoff rate (m^3/s), area$_{hru}$ is the hydrologic response uunit (hru) area (ha), K_{USLE} is the Universal Soil Loss Equation (USLE) soil erodibility factor, C_{USLE} is the USLE cover and management factor, P_{USLE} is the USLE support practice factor, LS_{USLE} is the USLE topographic factor and CFRG is the coarse fragment factor [*Williams*, 1995]. The peak runoff rate is calculated using:

$$q_{peak} = \frac{C * i * Area}{3.6} \qquad (4)$$

where C is the runoff coefficient, i is the rainfall intensity (mm/hr), and Area is the subbasin area (km^2). K_{USLE} describes the individual ability of soils to erode and is computed by:

$$K_{USLE} = \frac{0.00021 * M^{1.14} * (12 - OM) + 3.25 * (c_{soilstr} - 2) + 2.5 * (c_{perm} - 3)}{100} \qquad (5)$$

where M is the particle size parameters which is a function of percent silt, sand, and clay contents of the soil, OM is the percent organic matter (%), $c_{soilstr}$ is the soil structure code used in soil classification, and c_{perm} is the profile permeability class [*Wischmeier et al.*, 1971]. C_{USLE} is the ratio between soil loss caused by land cropped for specific conditions and loss from clean-tilled continuous fallow, computed by:

$$C_{USLE} = exp\left(\begin{array}{c} [ln(0.8) - ln(C_{USLE,min})] * \\ exp[-0.00115 * rsd_{surf}] + ln[C_{USLE,min}] \end{array} \right) \qquad (6)$$

where $C_{USLE,min}$ is the minimum value for the cover and management factor and rsd_{surf} is the residue on the soil surface (kg/ha) [*Wischmeier and Smith*, 1978]. P_{USLE} is the ratio between soil loss

resulting from a specific support practice, e.g., contour tillage, and the up-and-down slope culture. The default value implemented in SWAT is one. LS_{USLE} is the ratio between soil loss per unit area from a field slope and the soil loss from a 22.1 meter length of uniform 9% slope calculated by:

$$LS_{USLE} = \left(\frac{L_{hill}}{22.1}\right)^m * (65.41 * sin^2(\alpha_{hill}) + 4.56 * sin\, \alpha_{hill} + 0.065) \qquad (7)$$

where L_{hill} is the hill slope length (meters), m is a function of the HRU slope, and α_{hill} is the angle of the slope [*Williams*, 1995]. Finally CFRG is computed by:

$$CFRG = exp(-0.052 * rock) \qquad (8)$$

where rock is the percentage of rock in the first soil layer (%) [*Williams*, 1995]. SWAT has been extensively used in hydrologic studies including those that assess climate and LULC change impacts [*Gassman et al.*, 2007; *Johnson et al.*, 2012; *Krysanova and Srinivasan*, 2015; *R Wang et al.*, 2014].

5.2 Model Inputs

The SWAT model was prepared using ArcSWAT, an ArcGIS-ArcView extension and graphical user interface. Model development, calibration, and validation periods were from 1984 – 1989 and 1990 – 1994. Model inputs include spatially distributed LULC, digital elevation model, and soil maps. The watershed is delineated into subbasins and can then further be broken into hydrological response units (HRUs) for which the land use, topography, soil type and management practices may be assumed relatively homogeneous. HRUs aid in the simplification of simulations

and increase accuracy with regard to sediment loading as it can more appropriately capture plant diversity contained within a single subbasin [*Neitsch et al.*, 2011].

5.2.1 LULC

LULC data for 1992 was obtained from the National Land Cover Database (NLCD) and is shown in Figure 6 [*Vogelmann et al.*, 2001]. Full class names for the abbreviated land covers and their percentage of the watershed are provided in Table 2. The study region is primarily undeveloped and has minimal urban areas. Forested wetlands are prominent along the Apalachicola River and become more abundant, along with non-forested wetlands, closer to the mouth of the river. Agriculture and hay is typical of the northern region. There are heavily forested regions and significant range lands within the middle sections. Urban areas (low density, high density, and commercial) are minimal, having a combined area that makes up less than 1% of the total watershed. Wetlands account for 32% of the total watershed area while agriculture and hay coverage is around 20%. Forests are the most prevalent land coverage, making up 39% of the total area.
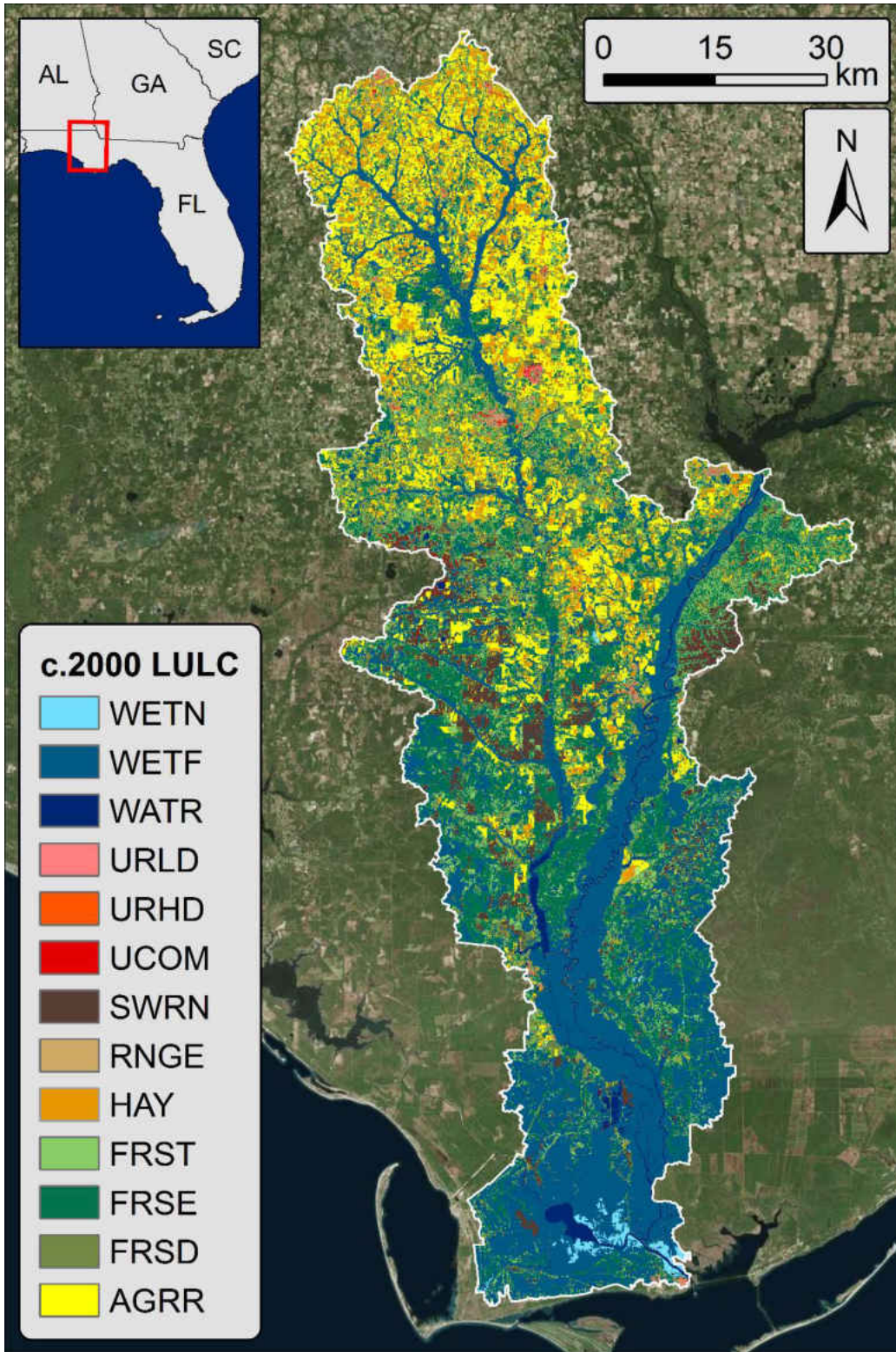
Figure 6 National Land Cover Database (NLCD) LULC c2000 within the study domain.
Full class names for each abbreviated land cover are provided in Table 2.

Table 2 c.2000 NLCD LULC class abbreviations, full name, and percentage of the watershed.

c.2000 Abbreviation	c.2000 full name	Percent of watershed
WETN	Wetlands – non-forested	0.70
WETF	Wetlands - forested	31.23
WATR	Water	1.97
URLD	Urban low density	0.49
URHD	Urban high density	0.04
UCOM	Commercial	0.27
SWRN	Southwestern US (Arid Range)	6.17
RNGE	Range - grasses	0.00
HAY	Hay	6.62
FRST	Forest - mixed	11.84
FRSE	Forest - evergreen	18.53
FRSD	Forest - deciduous	8.38
AGRR	Agricultural land-row crops	13.77

5.2.2 Digital Elevation Model

A digital elevation model (DEM) is comprised of topographic and bathymetric data. This study uses a DEM that was derived from online accessible, topographic data provided by the Northwest Florida Water Management District and surveyed bathymetry provided by the U.S. Army Corps of Engineers, Mobile District (http://www.nwfwmdlidar.com/). At 5 meter resolution, the extent spans from the bay to as far north as Marianna, FL. For the remaining part of the basin, 1/3 arc-second (~10 meter) resolution obtained from the National Elevation Dataset (NED) was used [*U.S. Geological Survey*, 2013]. These datasets were processed and combined using ArcGIS to develop a seamless DEM [*Medeiros et al.*, 2011] (Figure 7). Elevation and relief are relatively low near

the bay, where expansive wetlands are indicated by LULC data (Figure 6). Elevation increases moving north. The range is around -23 in the river to 110 meters referenced to NAVD88. Due to the fine resolution of the DEM, the Apalachicola and Chipola Rivers, as well as smaller tributaries throughout the domain are accurately captured.
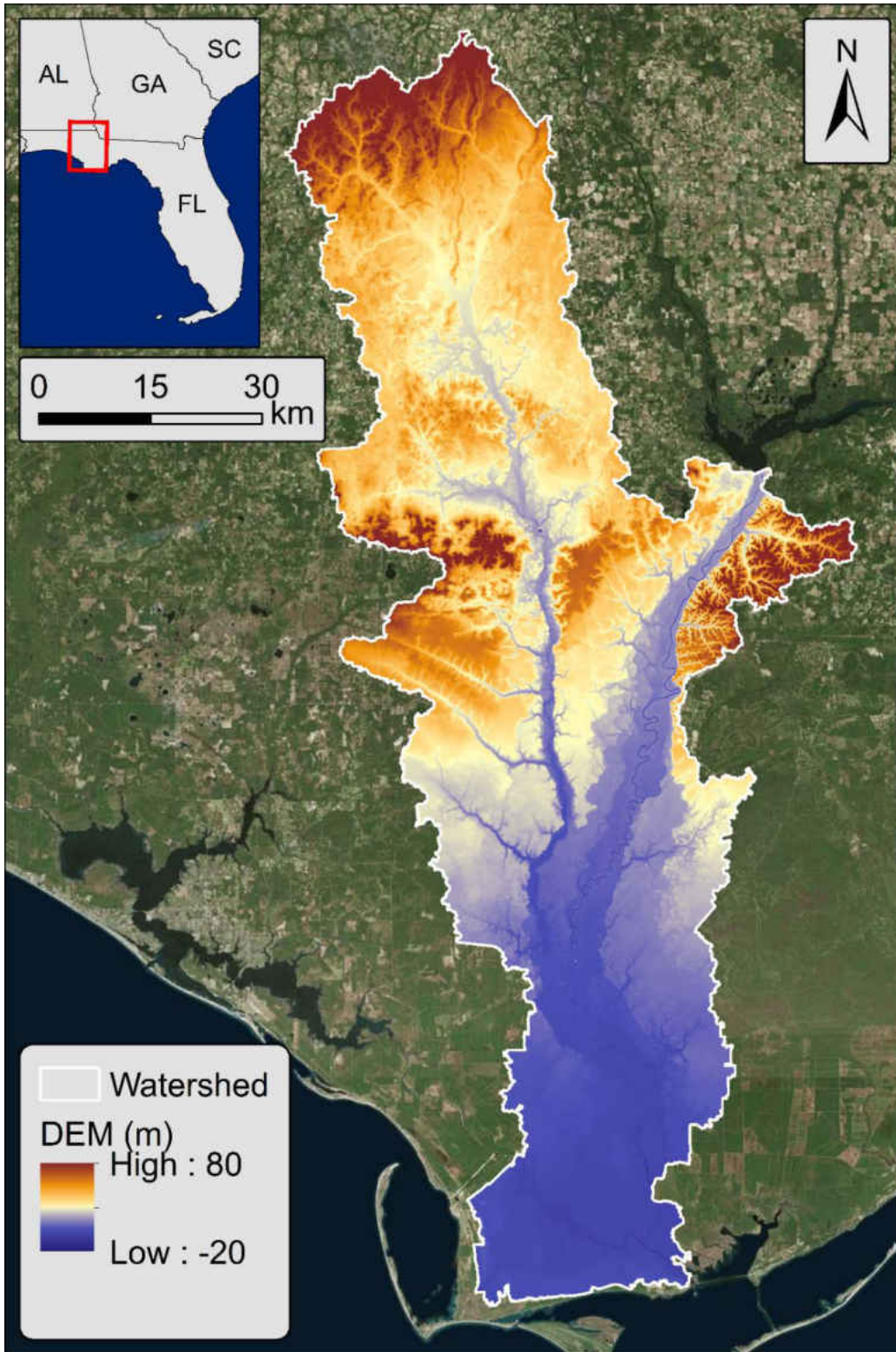
Figure 7 Digital elevation model (DEM) in meters (NAVD88) within study domain.

5.2.3 Soil

The soil data were acquired from the Soil Survey Geographic Database (SSURGO) [*US Department of Agriculture (USDA)*, 2007]. Data for the Florida counties: Bay, Calhoun, Franklin, Gadsden, Gulf, Jackson, Liberty, and Washington, Alabama counties: Geneva and Houston, and Georgia counties: Decatur were downloaded and merged within ArcGIS. Within ArcSWAT the code map unit MUKEY was used to merge individual units with soil attributes in the U.S. SSURGO Soils Database (http://swat.tamu.edu/software/arcswat/).

The hydraulic conductivity and percent of silt, sand, and clay are some of the physical properties that are defined by the SSURGO Soils Database. Values of hydraulic conductivity within the study domain range from 3 to 890 mm/hr with the lowest hydraulic conductivity, less than 10 mm/hr, seen along the floodplains of the Apalachicola River (Figure 8). Additionally, lower hydraulic conductivity is seen in the northern region near Dothan, AL. Sand is the most dominant soil type throughout the domain, with the exception along the Apalachicola River and surrounding floodplain (Figure 9). Along the river the percentage of silt and clay is larger and moving closer to the bay, the soil becomes mostly comprised of silt. It should be noted that the identifiable discontinuity in soil classification in the northern region of the domain occurs at the Florida – Alabama state line and is believed to be caused by differences in classifying / processing techniques by the states.
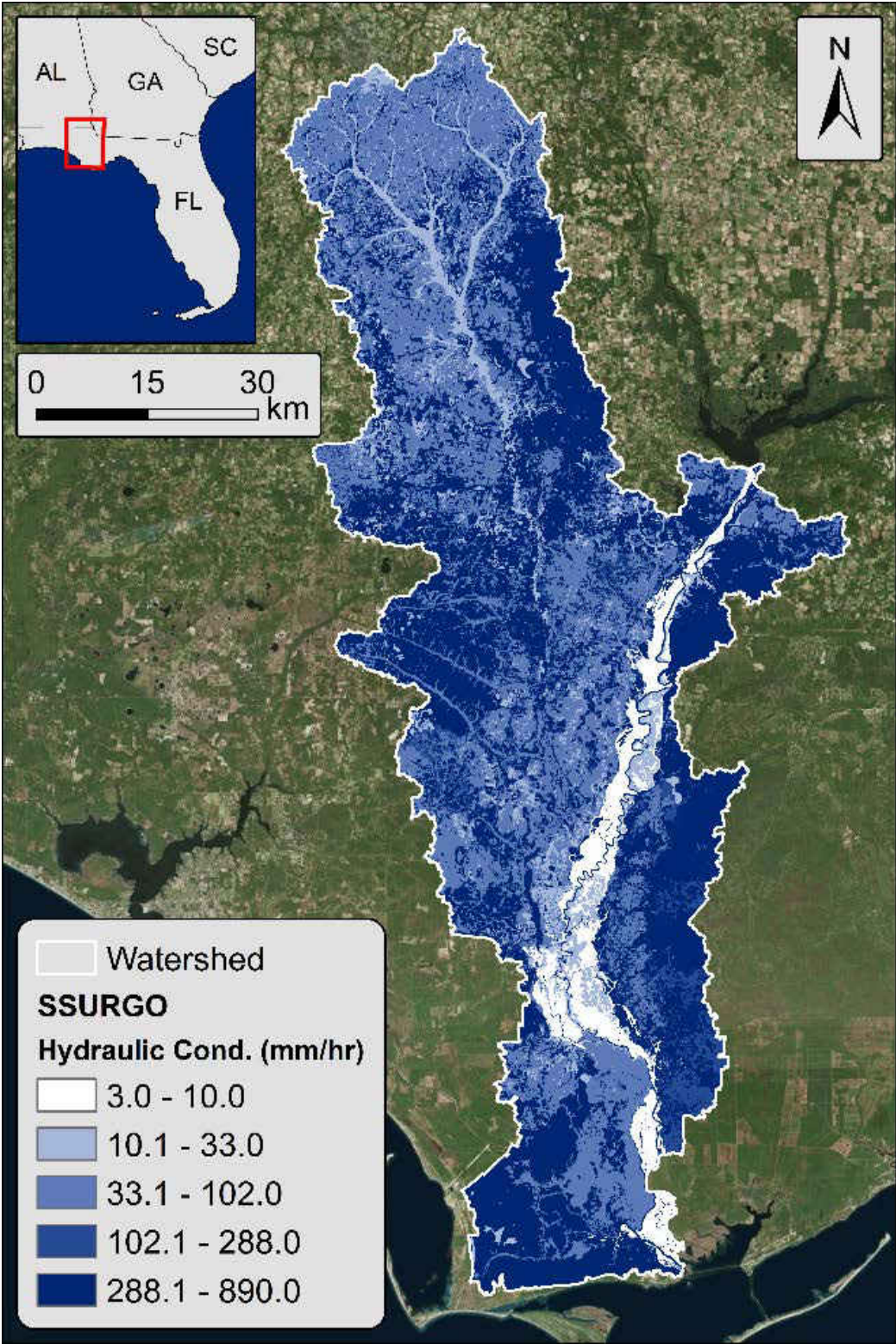
Figure 8 Hydraulic conductivity (mm/hr) of soils within the study domain.
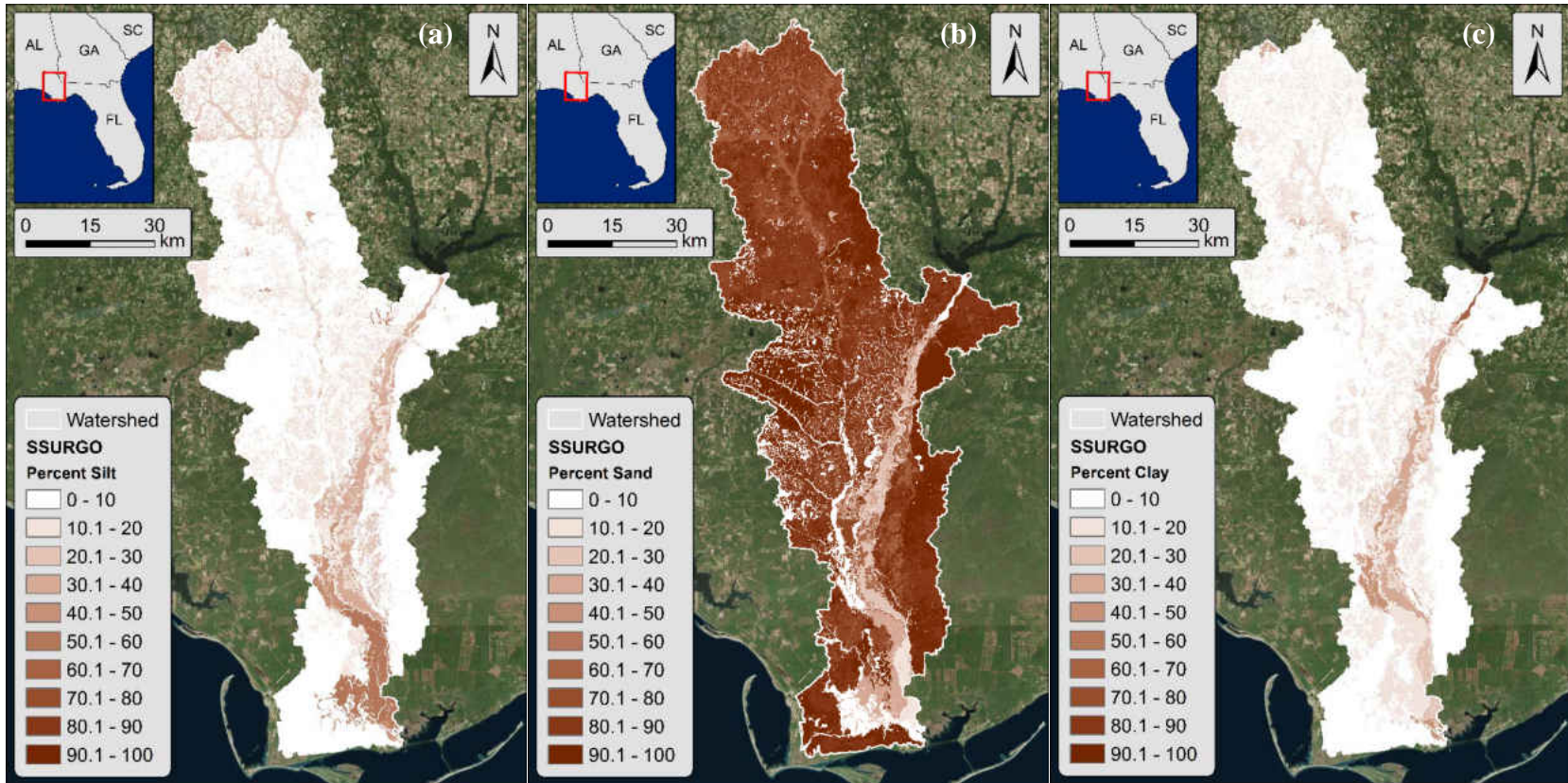
Figure 9 Percent (a) silt, (b) sand and (c) clay of soils within the study domain.

For each subbasin, a single or multiple HRUs can be assigned. In the case of multiple HRUs, which was the method selected for this study, user defined thresholds for land use, soil class and slope class are selected to guide discretization. This study applied a 5% threshold for each, meaning that land use, soils, and slopes that covered less than 5% of the subbasin area were eliminated and the remaining reapportioned. From the total 99 subbasins for the watershed, 4,187 HRUs were created.

5.2.4 Climate Data

SWAT climatic data includes precipitation, temperature, solar radiation, relative humidity, and wind speed. Observed daily data can be used singularly or in conjunction with a weather generator that creates values in place of missing data. The National Centers for Environmental Prediction (NCEP) developed the Climate Forecast System Reanalysis (CFSR) which provides weather data in SWAT file format [*National Centers for Environmental Prediction*, 2015]. Values from CFSR were generated for missing daily rainfall and temperature data and for all other climatic variables. Climatic data (precipitation and temperature) was downloaded for five stations (Table 3) from the National Centers for Environmental Information (NCEI) for 1/1/1984 – 12/31/1989 [*Menne et al.*, 2012]. This period will be referred to as the 'historic' period. The stations, as they are located in the study domain, are represented by the red circles in Figure 10.

Table 3 Climate station NCEI codes, downloaded data type, location, and elevations.

Station	NCEI Code	Data Type	Lat, Long (deg)	Elev (m)
Apalachicola Airport, FL	GHCND:USC00080211	Precip & Temp	29.72, -85.02	6.1
Wewahitchka, FL	GHCND:USC00089566	Precip & Temp	30.12, -85.20	12.8
Woodruff Dam, FL	COOP:089795	Precip	30.72, -84.87	23
Bristol, FL	COOP:081020	Precip	30.42, -84.99	48.8
Dothan, AL	COOP:012377	Precip	31.19, -85.37	83.8
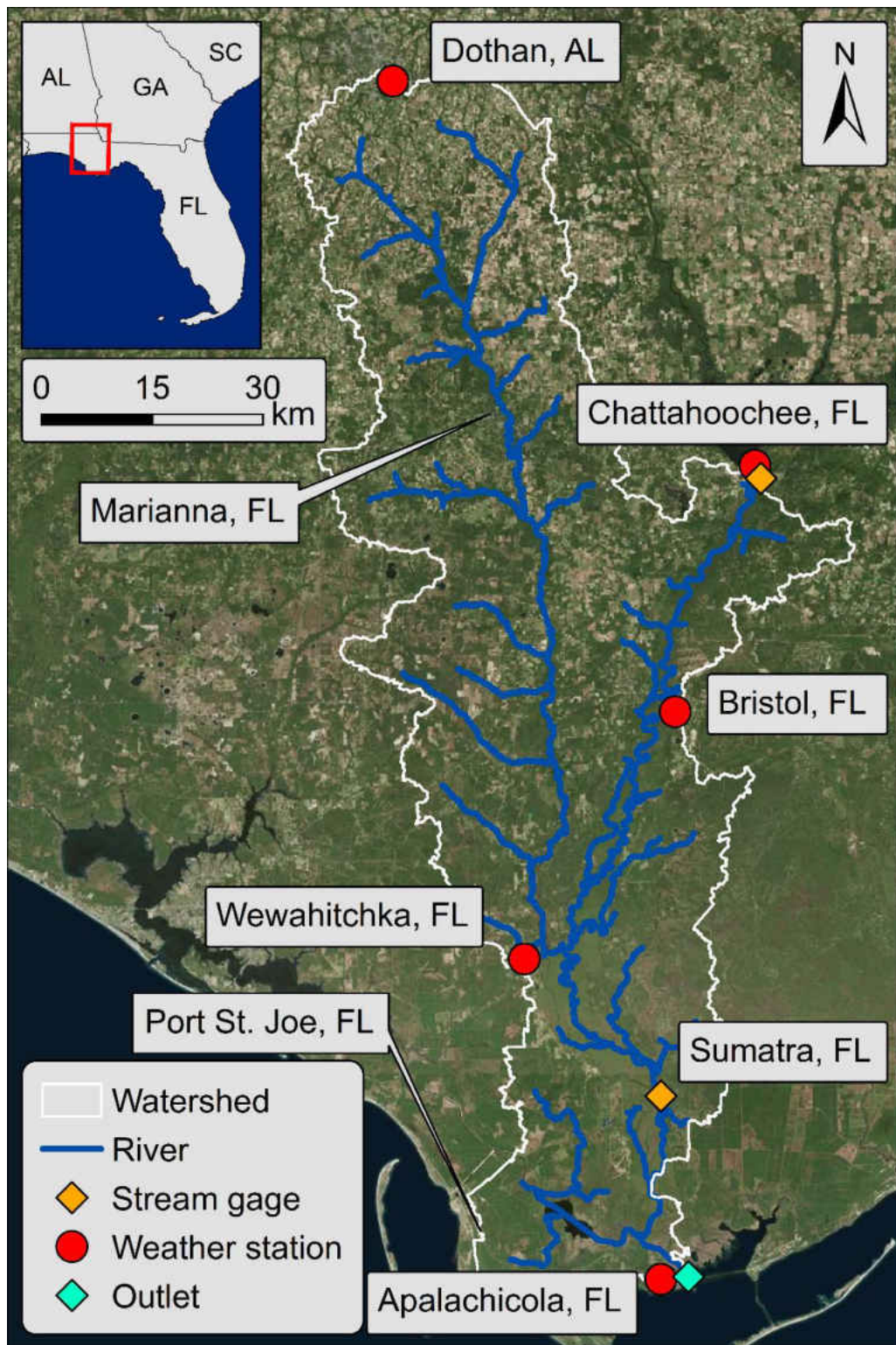
Figure 10 Location of stream gages (orange), weather stations (red) and outlet (cyan).

5.2.5 Boundary Conditions

The model applies one boundary condition for daily streamflow and sediment loading at the Jim Woodruff Dam. The boundary is applied at the same location as the U.S. Geological Survey (USGS) station 02358000 and is shown in Figure 10 by the orange diamond near Chattahoochee, FL [*USGS*, 2001]. Observed daily streamflow and sediment load were downloaded from the USGS station. Due to the limited number of observed sediment records occurring within the historic period, a power law regression analysis was performed between the observed daily streamflow and observed sediment load to establish a relationship that was used to derive an empirical sediment load.
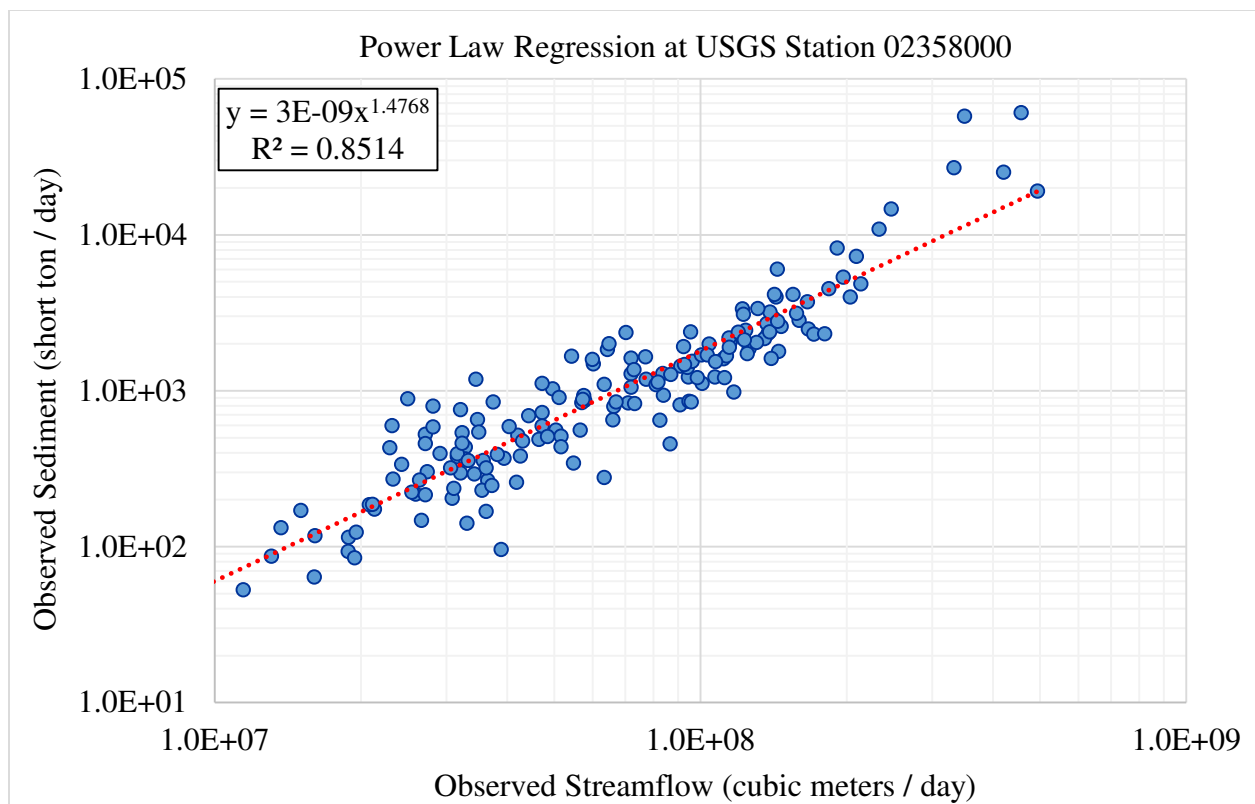
Figure 11 Power law regression analysis of sediment yield and stream flow at USGS 01247000 near Jim Woodruff Dam.

Several approaches were taken to develop the best fitting relationship. One method was to use multiple equations that would describe the data points at the extremes. Another was applying slight variations to the equation shown in Figure 11. The relationship that was finally implemented for this study was

$$sed_{empirical} = (3E - 9)Q_{observed}^{1.528} \qquad (9)$$

where $sed_{empirical}$ (tonnes/day) is the empirically derived daily sediment load and $Q_{observed}$ is the observed daily streamflow measured at USGS station 02358000 (m^3/sec). The empirically derived sediment load and observed streamflow were ultimately applied at the boundary. Observed daily values for streamflow and sediment load were also downloaded for a USGS station near Sumatra, FL (02359170), to be used for the model calibration / validation (Figure 10).

5.3 Assumptions and Limitations

The U.S. Army Corps currently regulates flow from the Jim Woodruff Dam and Lock. In the case of the future scenarios, the boundary conditions of streamflow and sediment load were assumed to remain unchanged from present conditions. Elevations and soil distributions were also assumed to remain constant from c.2000 to c.2100. In addition, tidal influences near the mouth of the river, while also important, are beyond the scope of this study.

5.4 Calibration and Validation

The model calibration and validation periods are 01/01/1985 – 12/31/1989 and 01/01/1990 – 12/31/1994, respectively. To reach stable conditions and avoid erroneous outputs, a one year ramp

55

up or warm up period was applied, therefore results from 1984 were excluded. The Nash-Sutcliffe efficiency (NSE) and percent bias (PBIAS) were used to assess the model's performance of daily output, with optimal scores being equal to 1 and 0, respectively. The Nash-Sutcliffe efficiency measures the residual variance to the variance of the observed data; an NSE equal to zero indicates the model predictions are as accurate as the measured data average and less than zero indicates the mean of the observed data is a better predictor than the model results [*Nash and Sutcliffe*, 1970]. Percent bias measures the model's average tendency to predict higher or lower values than the observed data; a positive PBIAS indicates the model tends to under predict values and a negative PBIAS indicates the model overestimation bias [*Gupta et al.*, 1999]. The NSE was the primary statistic used during the model calibration and the PBIAS served as a secondary measure.

Simulated results were compared with observed data from the USGS station near Sumatra, FL (02359170). Prior to any calibration, the streamflow NSE values for the calibration and validation periods were 0.57 and 0.43, respectively. The model was manually calibrated. Simulated sediment yield is reliant on the model's ability to capture surface runoff and peak discharge, therefore calibration of water quantity was made the primary focus. To help guide the process, a preliminary series of trials were run where parameters related to surface runoff, baseflow, and sediment yield were altered to their extreme values allowed by the model or believed to be scientifically defensible. The parameters that proved to affect model results most significantly were then categorized according to their main contribution to influence either streamflow or sediment quantity. Those parameters that affected both were grouped with the streamflow class. A second distribution broke up those parameters that altered streamflow into a primary and secondary hierarchy, based on the model sensitivity that was observed. The classification was then used to

develop the flow chart shown in Figure 12. The NSE calibration values shown in the red decision shapes were based on acceptable values found in the literature, the initial NSE values prior to calibration, and the sensitivity that was observed during the initial trial runs.

The list of the calibrated parameters, their descriptions, and adjusted values are listed in Table 4. The calibration adjustments with percentages describe the percent change of the parameter value from the original, default value. A single number reported for the calibration adjustment represents the ultimate value assigned for the parameter within the SWAT model.
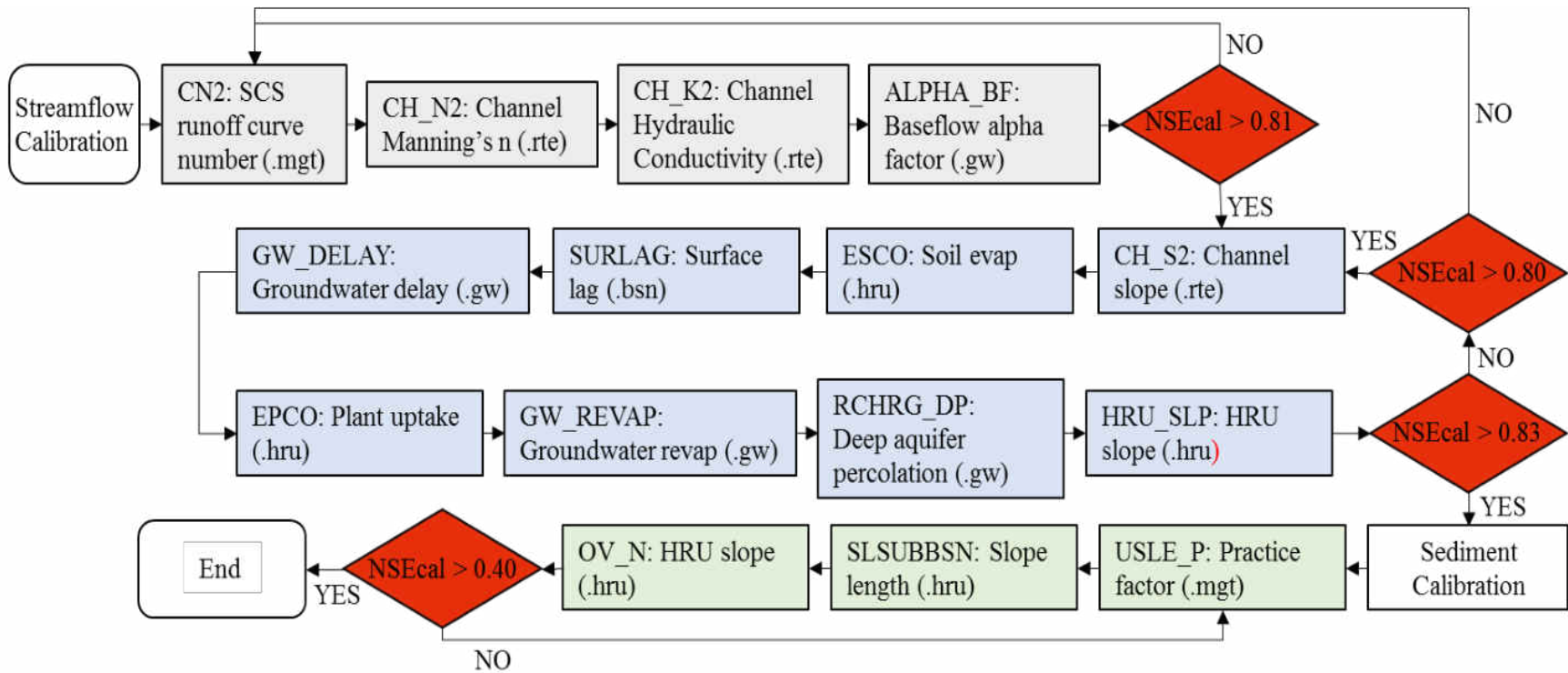
Figure 12 Calibration flow chart for streamflow and sediment loading.

Table 4 Calibrated SWAT parameters, descriptions, and adjustments.

Parameter	Description	Calibration Adjustment
CN2	SCS runoff curve number	-21.0%
CH_N2	Main channel Manning's "n"	0.019
CH_K2	Main channel effective hydraulic conductivity (mm/hr)	110
ALPHA_BF	Baseflow alpha factor (1/days)	0.25
CH_S2	Main channel average slope (m/m	+6.0%
ESCO	Soil evaporation compensation factor	0.75
SURLAG	Surface runoff lag coefficient	0.5
GW_DELAY	Groundwater delay time (days)	13
EPCO	Plant update compensation factor	0.54
GW_REVAP	Groundwater "revap" coefficient	0.2
RCHRG_DP	Deep aquifer percolation fraction	0
HRU_SLP	Average slope steepness (m/m)	-15.0%
USLE_P	USLE equation support practice factor	0.055
SLSUBBSN	Average slope length (m)	+50.0%
OV_N	Manning's "n" for overland flow	+50%

The model performance statistics are provided in Table 5. The calibration and validation NSE values for streamflow were 0.84 and 0.69 and the PBIAS was -2.42 and -9.32. The negative PBIAS indicates the model has an over prediction bias for the streamflow. While the boundary condition at the Jim Woodruff Dam applied the empirically derived sediment loading, the model sediment loading was calibrated and validated using observed data collected at USGS station. The calibration and validation NSE values for sediment loading were 0.42 and 0.44. The PBIAS for the sediment calibration period was 15.97 indicating an under estimation bias and for the validation

period the PBIAS was -29.74, indicating an over estimation bias. According to the literature and guidelines set by *Moriasi et al.* [2007], the model performance for both streamflow and sediment was determined above satisfactory, and can be considered good or very good for the application of daily time steps. The graphical time series of observed vs. simulated streamflow (m^3/s) and sediment load (tonnes/day) for both the calibration and validation periods are shown in Figure 12. The model adequately reproduces baseflow and events, both in magnitude and timing. Despite the difficulties often associated with modeling sediment, seasonal and event fluctuations are sufficiently captured by the model.

Table 5 Daily model performance statistics.

Statistic	Calibration		Validation	
	Streamflow	Sediment	Streamflow	Sediment
NSE	0.84	0.42	0.69	0.44
PBIAS	-2.42	15.97	-9.32	-29.74
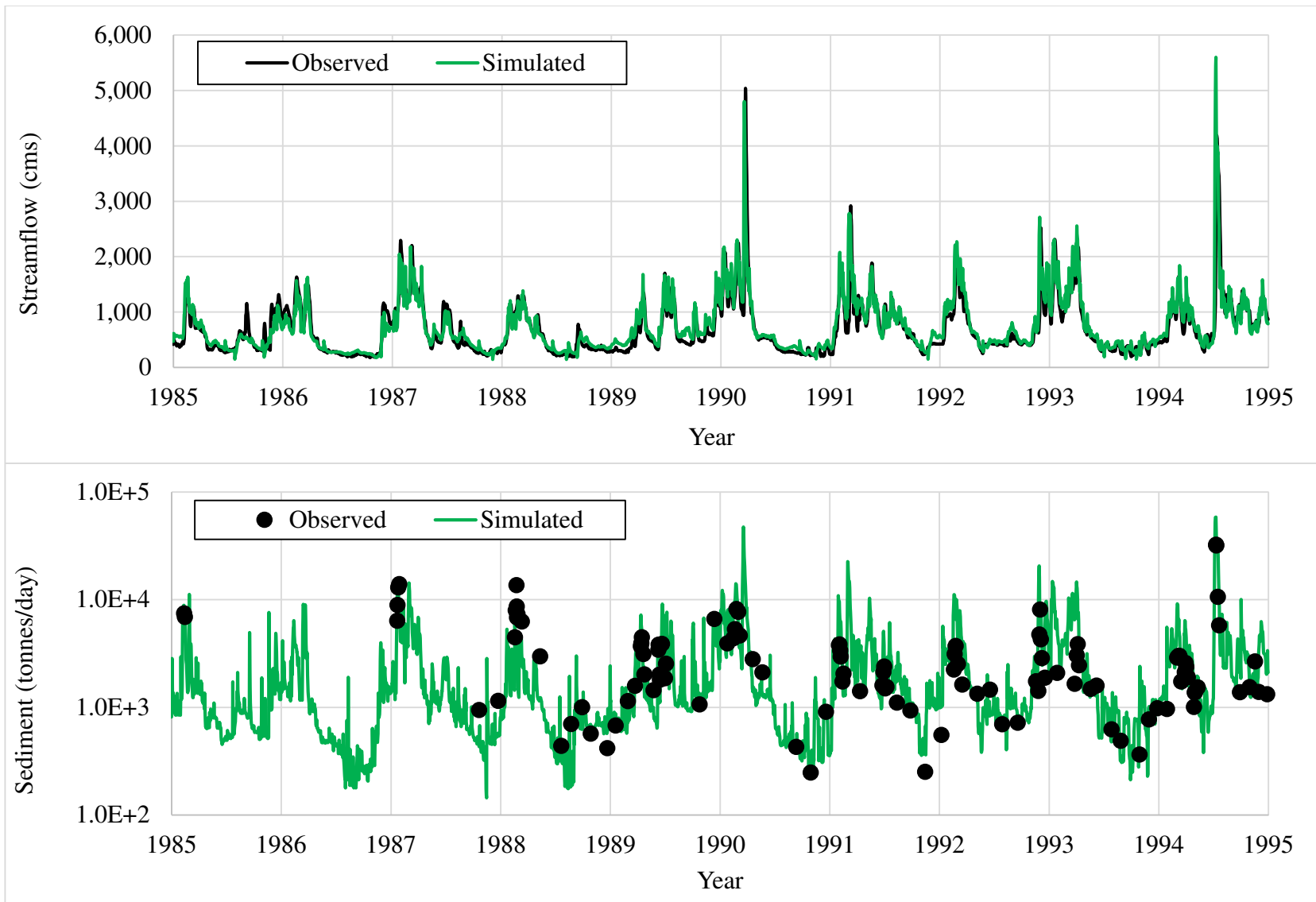
Figure 13 Observed vs. simulated time series for streamflow (cms) and sediment loading (tonnes/day).

CHAPTER 6: PROJECTED CLIMATE CHANGE

6.1 IPCC Special Report Emission Scenarios

Climate change projections refer to the Intergovernmental Panel on Climate Change (IPCC) Fourth Assessment Report (AR4). The AR4 is based on an ensemble of global climate model (GCM) outputs resulting from a collaborative effort made by several modeling groups worldwide [*IPCC*, 2007]. Future conditions impose A2, A1B, and B1 scenarios from the IPCC Special Report: Emissions Scenario (SRES), which represent potential future carbon emissions resulting from a range of driving forces (e.g., social, economic, environmental, technologic) [*IPCC*, 2000]. Briefly put, A2 describes a heterogeneous world, with uneven economic and technological growth and diversified social and political constructs. A1B describes a rapidly changing world with economic growth, population increase that then declines by 2100, and balance between supply sources and technological advancements. B1 is similar to A1B, describing a rapidly changing world with economic balance and but differs in that social and technological advancement is geared toward environmental conservation and sustainability. Fully described storylines for each scenario can be found in the IPCC-SRES [*IPCC*, 2000]

6.2 Global Climate Model Selection

While GCMs typically converge on global climate predictions, structural differences between GCMs can result in contradictory climate predictions at local scales [*Semenov and Stratonovitch*, 2010]. Further, specific GCMs have been shown to perform better for particular regions. *Cai et al.* [2009] assessed the performance of seventeen GCMs based on hindcasts of temperature and

precipitation for the periods of 1961 – 1990 and 1931 – 1960. Skill scores, based on the root mean square error (RMSE) for each GCM, ranging 0.00 – 0.06, 0.06 – 0.10, 0.10 – 0.20, and >0.20 were plotted globally on a 2° x 2° grid. The skill score as well as the model data availability to incorporate the maximum number of carbon emission scenarios guided the GCM selection process for this study. For a more comprehensive assessment, a multi-model inter-comparison approach was taken. The following three models were ultimately selected: (1) HadCM3 (HADCM3), (2) IPSL-CM4 (IPCM4), and (3) ECHAM5-OM (MPEH5) [*Semenov and Stratonovitch*, 2010]. The associated research centres and grid resolutions are provided in Table 6. The temperature skill score for each of the models fell in the 0.06 – 0.10 range. The precipitation skill score for IPCM4 and MPEH5 was 0.06 – 0.10 while HADCM3 ranged 0.10 – 0.20, indicating the HADCM3 may be more suitable for predicting future climate for this region.

Table 6 Selected global climate models, research centres, and grid resolutions [*Semenov and Stratonovitch*, 2010]

Global Climate Model	Model Acronym	Research Centre	Grid Resolution
HadCM3	HADCM3	UK Meteorological Office	2.5 x 3.75°
IPSL-CM4	IPCM4	Institute Pierre Simon Laplace	2.5 x 3.75°
ECHAM5-OM	MPEH5	Max-Planck Institute for Meteorology	1.9 x 1.9°

6.3 Downscaling Approach

Due to their coarse resolution, GCMs struggle to capture small scale processes that occur at local extents which can result in inaccurate climate predictions. What's more, GCMs often provide monthly averages or change rates, while many process based models, including SWAT, require

daily inputs. Various temporal and spatial downscaling techniques have been developed to resolve these issues including the implementation of weather generators. For this study, the Long Ashton Research Station-Weather Generator (LARS-WG) was used to generate daily, stochastic temperature and precipitation for the future climate change scenarios. LARS- WG is capable of producing daily, synthetic weather time series, i.e., baseline scenario, developed from and having the same statistical characteristics as localized, observed daily data. Similarly, future synthetic data can be generated for each carbon emission scenario, i.e., A2, and time period, i.e., 2081 – 2100, as predicted by the GCMs. Predictions from fifteen GCMs used in the AR4 have been built into the newest version of LARS-WG. Computed monthly changes between the baseline scenario and future synthetic dataset can then be incorporated into a scenario file (.sce) that is used by LARS-WG to perturb the baseline parameters, i.e., minimum / maximum temperatures and rainfall, at each grid point (Table 6). Data is interpolated across the study area between grid points using local and global interpolation procedures [*Semenov and Brooks*, 1999]. The final downscaled, daily climate data for temperature and rainfall is provided at each location for which the observed data was provided. For a more detailed description of LARS-WG and the downscaling approach applied, see *Semenov and Stratonovitch* [2010].

Thirty years of observed data, 1970 – 1999, from the above mentioned five weather stations previously shown in Figure 10, were used to create the baseline scenario representative of present day conditions. Weather was then generated under 2100 carbon emission scenarios (A2, A1B, and B1) as predicted by the GCMs (HADCM3, IPCM4, MPEH5) for the future conditions. The relative monthly change in precipitation and the absolute monthly change in temperature for each

scenario was incorporated into the scenario file and outputs provided the downscaled 2100 weather data used by SWAT.

Among the GCMs, there are stark dissimilarities in the relative change in rainfall (Figure 14). HADCM3 predicts wetter wet seasons and drier dry seasons. IPCM4 overall predicts a decrease in rainfall, with the exception of August and September. MPEH5 shows an increase in rainfall with the exception of August. The relationship among the carbon emission scenarios is variable with no one prevailing in more or less relative change to rainfall. On the other hand, the GCMs converge on the assumption that temperature will increase in this region from present to future conditions. HADCM3 has the largest absolute increase, particularly during the dry season. IPCEM4 is generally consistent throughout the year with little seasonal fluctuation, and MPEH5 shows an increase especially during May, June, October and November. In regard to the carbon scenarios, A2 shows a dominant increase in temperature to all other scenarios. A1B is secondary and the B1, while still showing an increase, is drastically smaller than A2 and A1B.

Figure 14 Monthly relative change in rainfall (a) HADCM3, (b) IPCM4 (c) MPEH5 and absolute change in temperature (°C) (d) HADCM3 (e) IPCM4 and (f) MPEH5 from present to future.
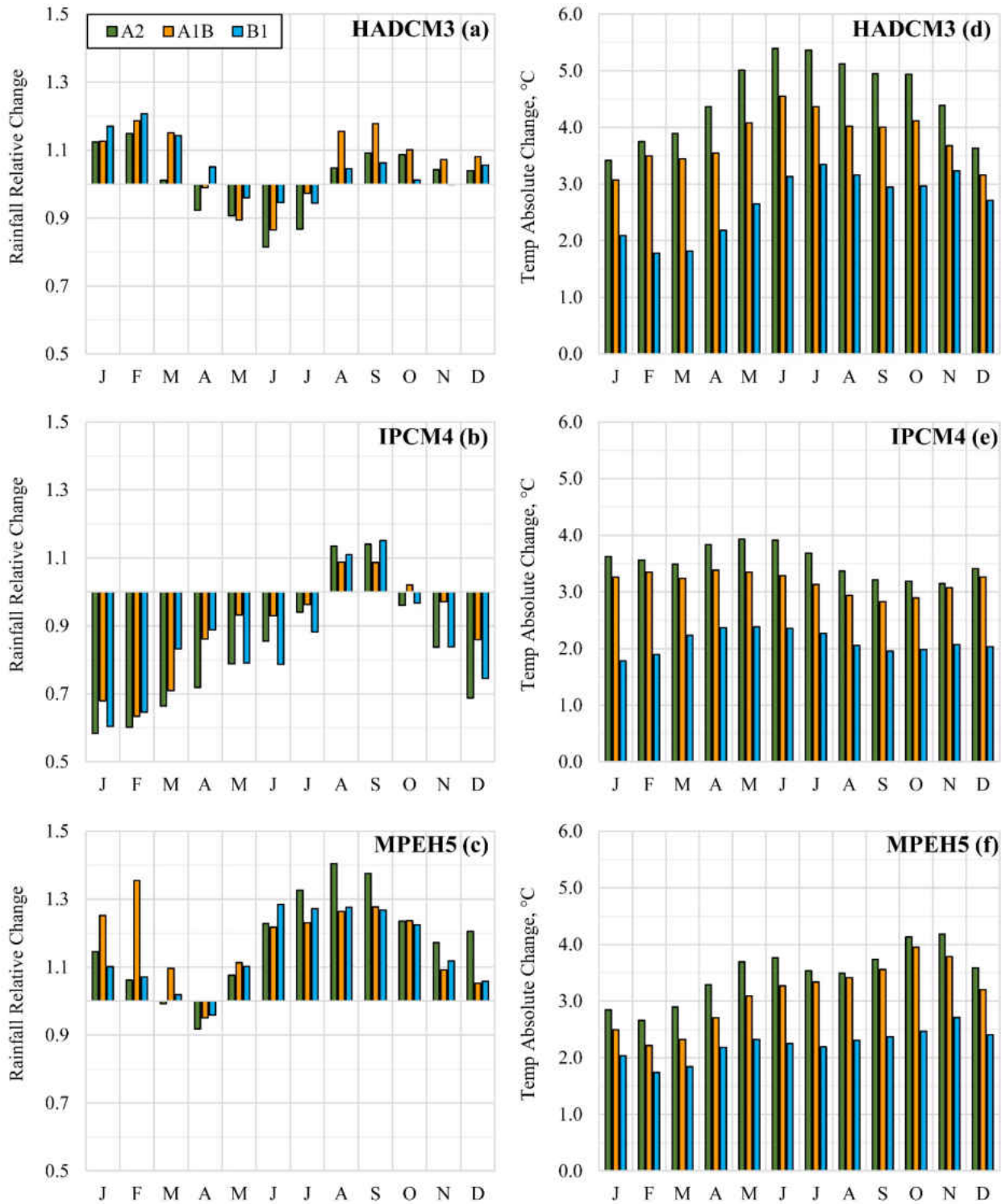
CHAPTER 7: PROJECTED LAND USE LAND COVER CHANGE

In keeping with future IPCC carbon emission scenarios, projected 2100 A2, A1B, and B1 LULC provided by the United States Geological Survey (USGS) EROS Center was selected to asses LULC change impacts [*USGS EROS Center*, 2014]. The maps were developed by incorporating data from each SRES into a spatially explicit model. Some land cover classes in the 2100 LULC are incongruent with those recognized by SWAT in the land cover lookup tables and were therefore adapted in a way that datasets could be incorporated into the SWAT model and were comparable with present day (c.2000) classifications. The 2100 classes and their updated c.2000 class assignment are shown in Table 7.

Table 7 Adaptation of 2100 to c.2000 LULC classes

2100 original	2100 adapted	Abbreviation for 2100 adapted
Herbaceous wetland	Wetlands - nonforested	WETN
Woody wetland	Wetlands - forested	WETF
Water	Water	WATR
Developed	Urban high density	URHD
Mining	Southwestern US range	SWRN
Barren	Southwestern US range	SWRN
Grassland	Range - grasses	RNGE
Mechanically disturbed national forest	Forest - mixed	FRST
Hay / pasture land	Hay	HAY
Mechanically disturbed other public lands	Forest - mixed	FRST
Mechanically disturbed private	Forest - mixed	FRST
Mixed forest	Forest - mixed	FRST
Shrubland	Forest - mixed	FRST
Evergreen forest	Forest - evergreen	FRSE
Deciduous forest	Forest - deciduous	FRSD
Cropland	Agricultural land-row crops	AGRR
Perennial ice / snow	--	--

The spatially distributed maps for the future 2100 A2, A1B, and B1 are shown in Figure 14 and the percentage of the study domain for each land cover type is listed in Table 8. From present to 2100 A2, forests yield to agriculture, a 109% increase, and urban areas, particularly Dothan, AL, Marianna, Wewahitchka, Port St. Joe and Apalachicola, FL, are predicted to increase. The relative offsetting of sediment-producing land uses such as urban and agriculture by sediment-conserving forests is expected to increase sediment yield for the A2 LULC class compared with present day conditions. A1B shows an increase in urban area with less emphasis near the coast for Apalachicola and Port St. Joe and less new agricultural area as compared to A2. The A1B is most similar to the present conditions in regard to cumulative land allotted for urban, agriculture, and forest. B1 shows similar urban development as A1B, however there is a 31% decrease in agriculture as it gives way to forested area, which is expected reduce the total sediment yield. From c.2000 to 2100 wetlands, both forested and non-forested, remain fairly consistent. The changes occurring within the 2100 LULC sets align with the fundamental storylines developed by the SRES for which they are based on.
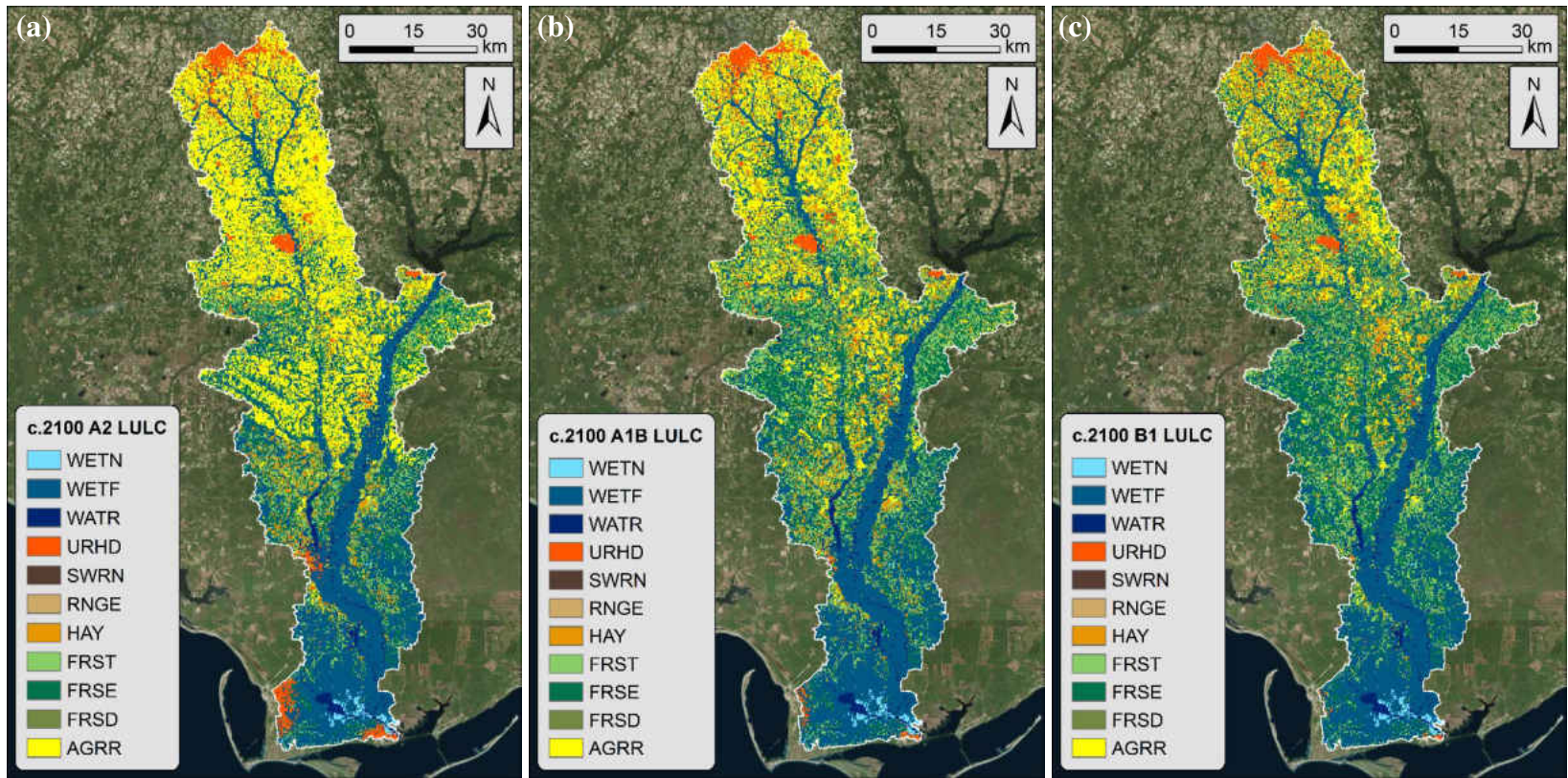
Figure 15 LULC for 2100 (a) A2, (b) A1B, and (c) B1. 2100 classes have been adapted to match c.2000. Full class names for each abbreviation are provide in Table 6.

Table 8 Percentage of land cover type in study domain for each LULC dataset

LULC	c.2000	2100A2	2100A1B	2100B1
WETN	0.7	0.7	0.7	0.7
WETF	31.2	30.6	31.2	31.5
WATR	2.0	2.0	2.0	2.0
URLD	0.5	0.0	0.0	0.0
URHD	0.0	3.7	2.6	1.8
UCOM	0.3	0.0	0.0	0.0
SWRN	6.2	0.0	0.1	0.0
RNGE	0.0	0.0	0.0	0.0
HAY	6.6	6.2	8.4	7.6
FRST	11.8	10.2	15.8	16.4
FRSE	18.5	14.1	17.5	22.5
FRSD	8.4	3.6	6.1	8.0
AGRR	13.8	28.9	15.6	9.5

CHAPTER 8: ASSESSMENT OF CLIMATE AND LAND USE LAND COVER IMPACTS

8.1 Simulation Ensemble

Following is the assessment of streamflow and sediment response to changes in (1) climate, (2) LULC, and (3) coupled climate and LULC change. Outputs are evaluated near the mouth of the river outside the bound of tidal influence prior to entering Apalachicola Bay as indicated by the cyan colored diamond in Figure 10. When assessing the seasonal response of climate and LULC change, streamflow and sediment that are applied at the Jim Woodruff Dam boundary are excluded; daily influx values have been subtracted from the daily output values at the outlet prior to analysis. This is done to further target alterations originating in the study domain and highlight changes that might otherwise be diluted by incorporating the total flow. The baseline simulation represents present day conditions and serves as the constant to which the future simulations' predictions are compared.

Table 8 shows the total simulation ensemble detailing the climate and LULC implemented for each. In the case of climate only, data are presented for each carbon emission scenario (A2, A1B, and B1) as predicted by each GCM (HADCM3, IPCM4, and MPEH5) and LULC represents present day conditions. There are a total of nine simulations for this category. For LULC only, climate is representative of present day and 2100 LULC for each carbon scenario is simulated, making for a total of three simulations. Incorporating coupled climate and LULC change, a total of nine simulations capture the carbon scenarios for each GCM and corresponding 2100 LULC.

Table 9 Simulations and applied climate / LULC conditions.

Description Conditions	Simulation	Climate (Scenario – GCM)	LULC
Baseline	1	Present (c.2000)	c.2000
Climate Only	2	A2 - HADCM3	c.2000
	3	A1B - HADCM3	
	4	B1 - HADCM3	
	5	A2 – IPCM4	
	6	A1B - IPCM4	
	7	B1 – IPCM4	
	8	A2 – MPEH5	
	9	A1B – MPEH5	
	10	B1 - MPEH5	
LULC Only	11	Present (c.2000)	2100 A2
	12	Present (c.2000)	2100 A1B
	13	Present (c.2000)	2100 B1
LULC and Climate	14	A2 - HADCM3	2100 A2
	15	A1B - HADCM3	2100 A1B
	16	B1 - HADCM3	2100 B1
	17	A2 – IPCM4	2100 A2
	18	A1B - IPCM4	2100 A1B
	19	B1 – IPCM4	2100 B1
	20	A2 – MPEH5	2100 A2
	21	A1B – MPEH5	2100 A1B
	22	B1 - MPEH5	2100 B1

8.2 Streamflow and Sediment Yield Response to Climate Change Only

The average, monthly runoff (cms) and sediment loading (tonnes / day) were used to compare quantities and seasonal shifts from present (baseline) to future (Figure 16). The future simulations include changes to climate only as predicted by each GCM. Results for each GCM are assessed individually and general behaviors that are in agreement for each GCM are summarized.
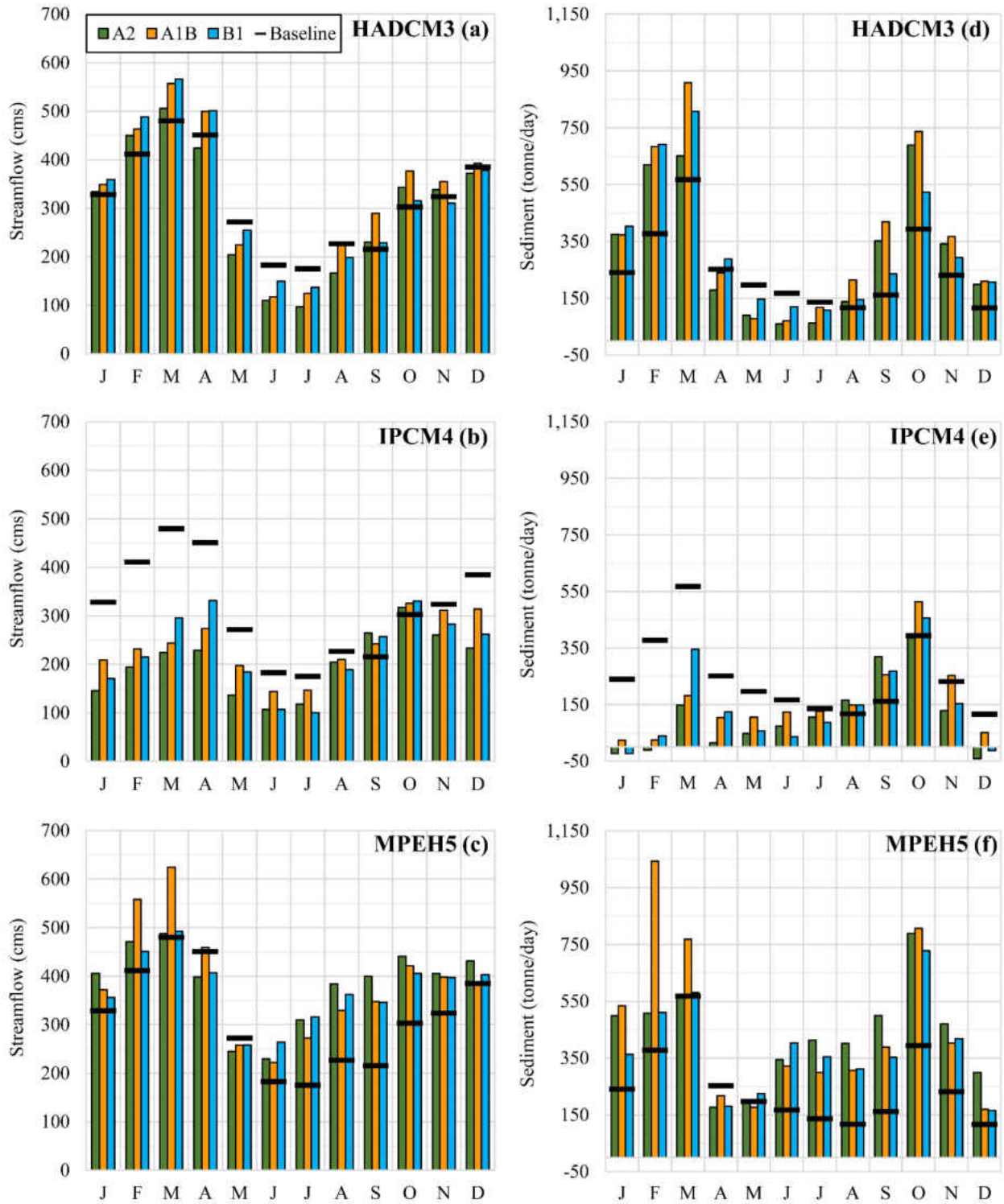
Figure 16 Monthly average streamflow (cms) for (a) HADCM3, (b) IPCM4 (c) MPEH5 and sediment (tonnes / day) (d) HADCM3 (e) IPCM4 and (f) MPEH5. The colors represent baseline (black), A2 (green), A1B (orange) and B1 (blue). Only climate change is considered.

8.2.1 HADCM3

HADCM3 predicts a more heterogeneous seasonal pattern than the baseline, with higher high flows (near January – April and September - November) and lower low flows (May – August). This pattern is closely correlated with the relative change in rainfall (Figure 14(a)). For the majority of the year, the A2 scenario produces lower runoff than A1B and B1. The highest runoff is predicted by B1 during the earlier months of the year (January – July) and then a shift occurs in the later months (August – December) when A1B is highest. Compared to the baseline, future sediment will be amplified during high loading periods and decreased during low loading periods. In general, when streamflow is predicted to increase or decrease from present to future, sediment mirrors the behavior. The exceptions to this trend occur later in the year (August – December) when sediment is predicted to increase despite some flow decreases for the A2 and B1 scenarios (Figure 16(d)). The relationship between runoff and sediment is also nonlinear. An example of this is seen for March when the A1B estimates a 60% increase in sediment loading relative to a 16% increase in runoff.

8.2.2 IPCM4

IPCM4 forecasts a future decrease in runoff for all months and carbon scenarios, with the exception of September and October (Figure 16(b)). The average monthly flows are more homogenous throughout the course of the year, similar to the absolute temperature increase for IPCM4, which had smoother seasonal transitions compared to other GCMs (Figure 14(e)). Patterns emerging between the carbon scenarios are difficult to distinguish, though A1B tends to be higher than A2 and B1 during the drier, summer months. Near the wet season from January – May there was an average percent reduction of 54%, 43%, and 45% from the baseline to future for A2, A1B, and

74

B1, respectively. Regarding the sediment loading, negative values in January, February, and December for A2 and A1B indicate more sediment is coming into the study domain at the Chattahoochee inlet than is exiting into the Bay (Figure 16(e)). This implies sediment is settling or being deposited within domain before reaching the outlet. There is also an estimated increase of loading during the months of August – October. As with the flow, A1B tends to estimate higher values than A2 and B1 for the majority of months out of the year.

8.2.3 MPEH5

MPEH5 indicates runoff may increase, particularly during later months of the year (June – December) with A2 estimating the largest quantities (Figure 16(c)). Earlier in the year during February and March, A1B is the dominant scenario and increases by 36% and 30%, respectively. In correspondence with this, the sediment loading also drastically increases 177% and 36% (Figure 16(f)). Within the wet seasons, A1B has the largest loadings and during the dry season, A2 is typically largest. Minimum loadings are predicted by the MPEH5 model to occur in April and May.

8.2.4 Convergence of Global Climate Models

The dissimilarities in response to climate change as predicted by the GCMs highlight the structural differences that exist between each model. Still, some general trends can be extracted where outputs are in agreeance for all three GCMs. The GCM ensemble converges on streamflow and sediment loading increasing in September and October for each scenario. With the accompanied flow, sediment loading will also be increased for these months. Further, loading for the baseline

is at its minimum from July to September, however future minimal values occur earlier in the year

near April to June.

8.3 Model Response to Land Use Land Cover Change Only

Figure 17 shows the average monthly flow and sediment loading under future LULC change only

for each carbon emission scenario compared to the baseline. Runoff is virtually unaltered by the

changes made to land use; future quantities match the present baseline with monthly differences

equaling no more than ± 20 cms, occurring from August – October. Sediment loading is more

significantly affected, with monthly averages differing from the baseline ± 185 tonnes / day (Figure

17(b)). Further, a distinct response to the specific carbon scenarios is more easily identifiable. A2

predicts an increase in loading for all months. The largest increase (33%) occurs in March. A1B

produces similar monthly averages compared to the baseline, and B1 results in a decrease in

sediment loading. The largest deviation between the baseline and B1 also occurs in March, when

the sediment loading is projected to reduce by 18%. Over the course of the entire 30 year

simulation, the sediment percent change for A2, A1B, and B1 from the baseline are +43.8, -0.4,

and -20.8, respectively. Percent change for runoff is < 1% for all three scenarios. In general, the

seasonal fluctuations of future streamflow and sediment loading remain consistent with present

day conditions.
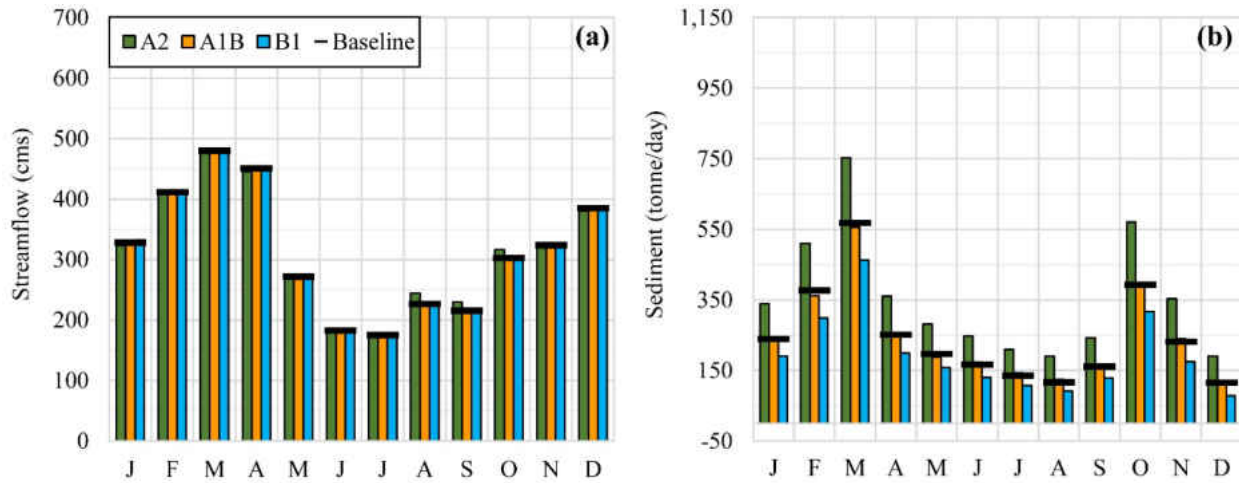
Figure 17 Monthly average (a) streamflow (cms) and (b) sediment (tonnes / day). The colors represent baseline (black), A2 (green), A1B (orange) and B1 (blue). Only LULC change is considered.

8.4 Model Response to Coupled Climate and Land Use Land Cover Change

The coupling of both future climate and LULC change was simulated for each GCM and monthly averages for runoff and sediment loading are shown in Figure 18. The general behaviors of increasing or decreasing from the baseline to the future are similar to the changes in climate only simulations, both seasonally and for individual months. Therefore, subtle differences observed by the coupling of climate and LULC change as opposed to applying one or the other are assessed. The object was to assess if changes in one would exacerbate or dampen the effects of the other. To do so, the deviations from the baseline to future for climate only, LULC only, and coupled climate and LULC are evaluated as they relate to one another.

77
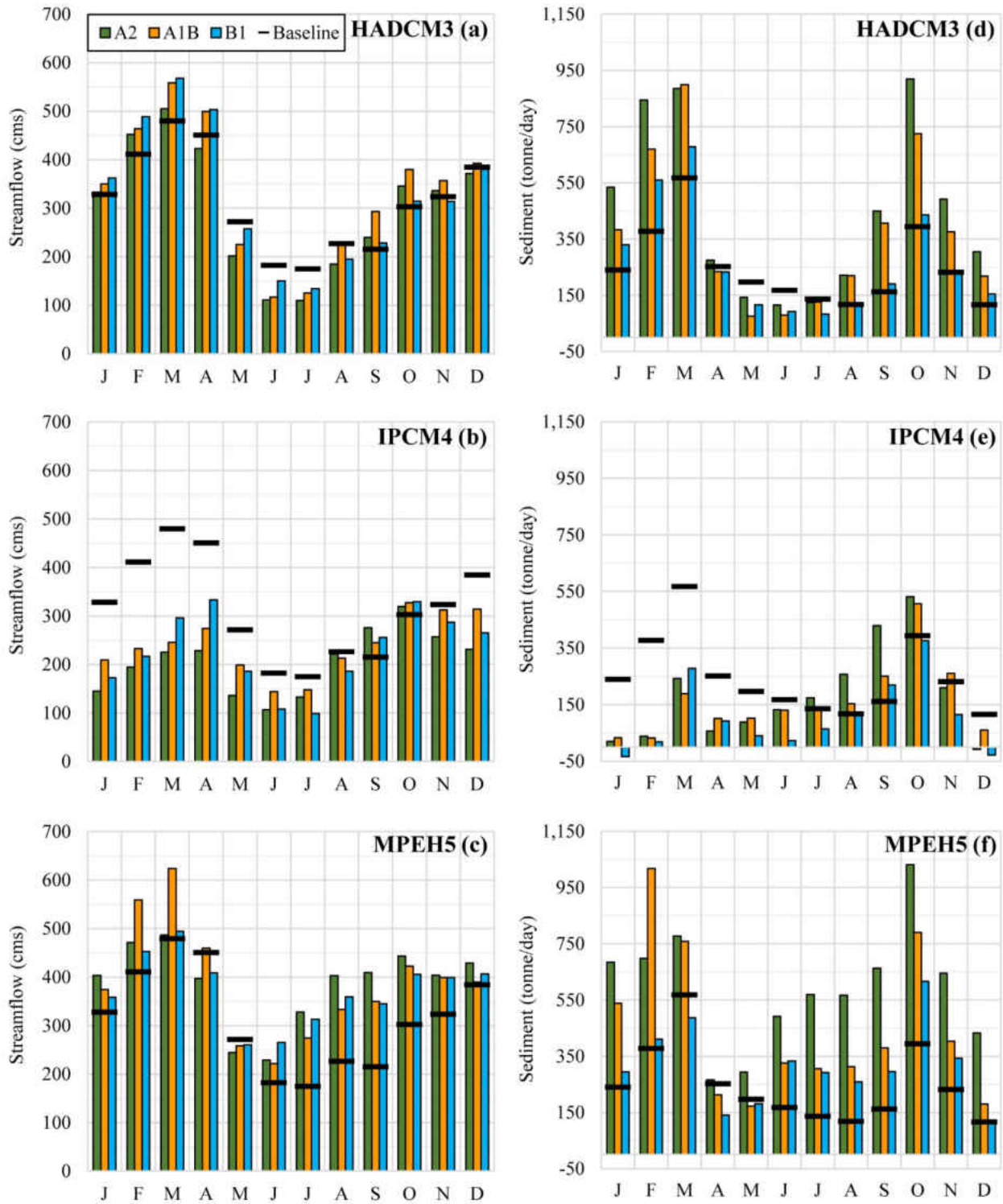
Figure 18 Monthly average streamflow (cms) for (a) HADCM3, (b) IPCM4 (c) MPEH5 and sediment (tonnes / day) (d) HADCM3 (e) IPCM4 and (f) MPEH5. The colors represent baseline (black), A2 (green), A1B (orange) and B1 (blue). Climate and LULC change is considered.

8.4.1 Runoff

Overall, modeled runoff is nearly unmoved by the coupling effect as compared to the climate only simulations, which reemphasizes the minimal effect of LULC change on flow for this particular study. When both climate only and LULC only simulations estimated an increase in runoff from the baseline, the additive quantities resulted in a value that was greater than predicted when the two were coupled during the simulation. For example, September A2 – HADCM3 flow is predicted to increase from the baseline by 14 cms for both the climate only and LULC only simulations, which combined would equal a 28 cms increase. However, coupling the two results in only a 24 cms increase from the baseline. Alternatively, for A2 in June and July when runoff was predicted to decrease for climate only and LULC only simulations, the coupled climate and LULC change resulted in a smaller reduction from the baseline.

8.4.2 Sediment Loading

A more dynamic interaction occurs in the response of sediment loading and nonlinearities resulting from the coupling of climate and LULC change are more detectable. All models indicate sediment increase may be amplified by the coupled interaction when both climate only and LULC only simulations predict an increase, e.g. October A2 – HADCM3, November A1B – IPCM4, and August A2 – MPEH5. When both climate and LULC are predicted to decrease from the baseline independently (April B1 – MPEH5 and June B1 – HADCM3) the combined interaction causes less of a decrease from the baseline than would be estimated by superposition. In the instance when the loading for LULC only decreases and climate only increases (March A1B – HADCM3), sediment may result in larger values compared to a linear response. Conversely, when LULC only increases and climate only decreases, e.g. April A2 – MPEH5 and February A2 – IPCM4, loadings

may be predicted as having overall lesser values than expected if the incremental increase / decrease from the baseline for isolated climate and LULC change simulations were added.

8.4.3 Dynamic Response Case Study

The monthly streamflow and sediment loading response to coupling changes in climate and LULC was further assessed for the HADCM3 model to evaluate if the processes might be modeled as isolated occurrences or if the interaction could result in a dynamic, non-linear response. To do so, the deviations from the baseline for the climate only, LULC only, and climate and LULC simulations were plotted (Figure 19 (a), (b), and (c)). To test if the simulated response to climate and LULC might be represented by modeling these processes separately and then estimated using methods of superposition, the additive deviation quantities for the climate only and LULC only simulations were then subtracted from the climate and LULC simulation (Figure 19(d)). A value of zero represents a linear response. A value greater than zero indicates a dynamic response where deviations from the baseline, regardless of being an increase or decrease, would be larger by simulating climate and LULC simultaneously in the model that was predicted using the results for the additive individual responses. A values less than zero still indicates a dynamic response but one where the coupled climate and LULC change simulation predicted less of a deviation from the baseline for future conditions than would be estimated by the individual processes.

Figure 19(d) shows near zero, positive, and negative values for the individual carbon emission scenarios. A2 shows the coupling effect of climate and LULC changes may result in amplified response for the early months of the year (January – July) as well as for December while a dampened response was observed for August – November. A polar response to the monthly

behavior seen for A2 was detected for the B1 scenario, while A1B was relatively close to zero differing no more that ±5 cms, suggesting the scenario may be predicted by superposition.

Figure 19 Future streamflow deviations from the baseline for HADCM3 the A2 (green), A1B (orange) and B1 (blue) scenarios. (a) Climate only, (b) LULC only, (c) climate and LULC, and (d) deviations climate and LULC – (deviations climate only + deviations LULC only)

The same analysis was performed for the sediment loading (Figure 20). A dynamic response to the coupled interaction of climate and LULC change was observed for the sediment loading. For the A2 carbon scenario, response is amplified for the months of January – March and August –

December while during the summer months a de-amplification is shown. The seasonal behavior aligns with those observed by the climate only simulation, with sediment predicted to increase for all months with the exception of April – July. This indicates that the coupling effect may predict larger quantities of sediment loading that would be suggested by the modeling climate and LULC changes separately. As seen with the streamflow, the A1B scenario is relatively small and might be estimated by superposition. Further as with the streamflow, behavior experienced by the B1 scenario is typically opposite, in regard to being positive or negative, to A2. The seasonal fluctuation appears to be driven by changes in climate and that by incorporating both changes, sediment loading of B1 is made closer to the baseline. That is, in instances where the climate only simulation predicted an increase in loading, the response was dampened, and when loading was predicted to decrease (summer months), the deviations from the coupled simulations were enlarged. The behavior observed suggests a dynamic response for both streamflow and sediment loading to coupling changes in climate and LULC within the model simultaneously.
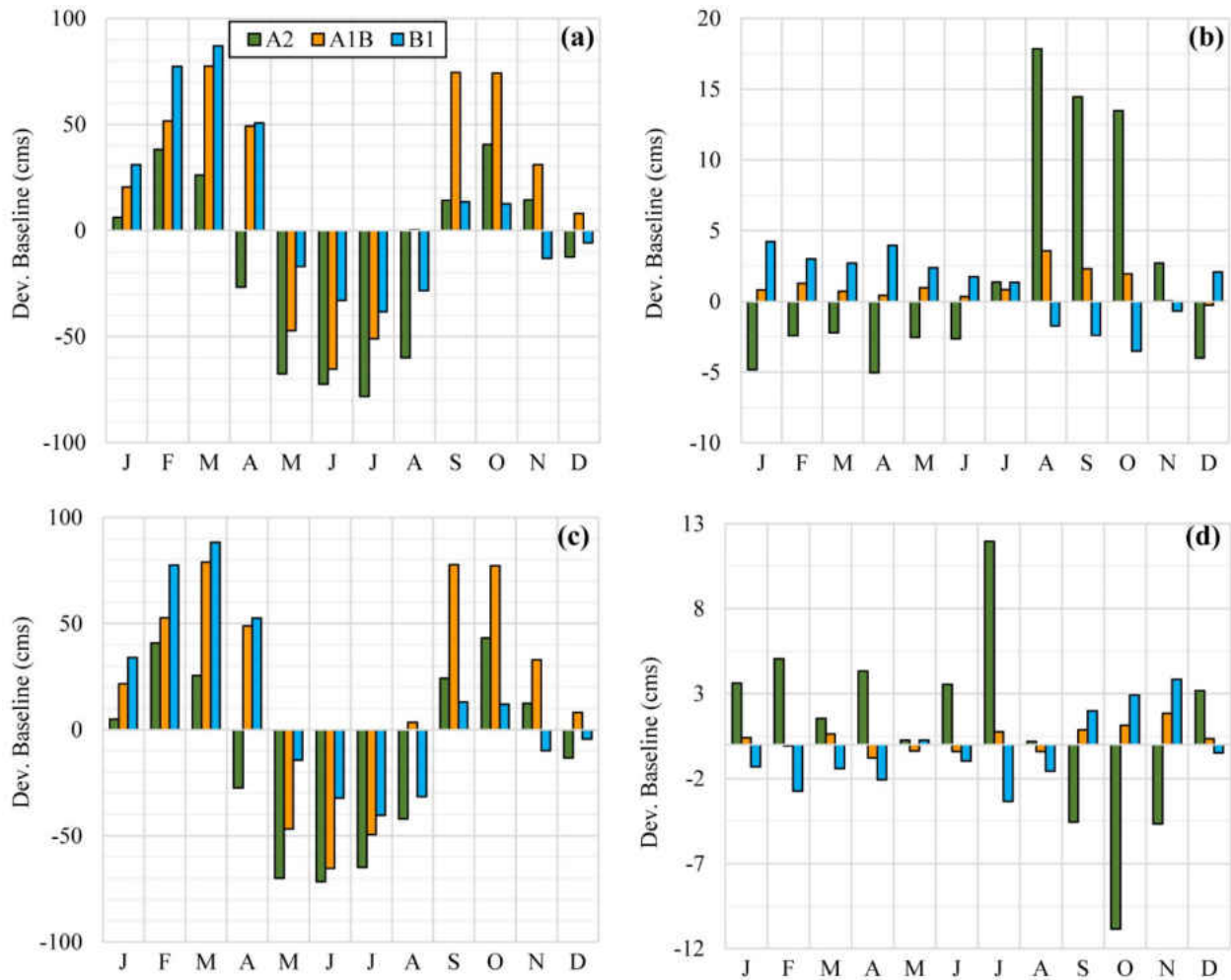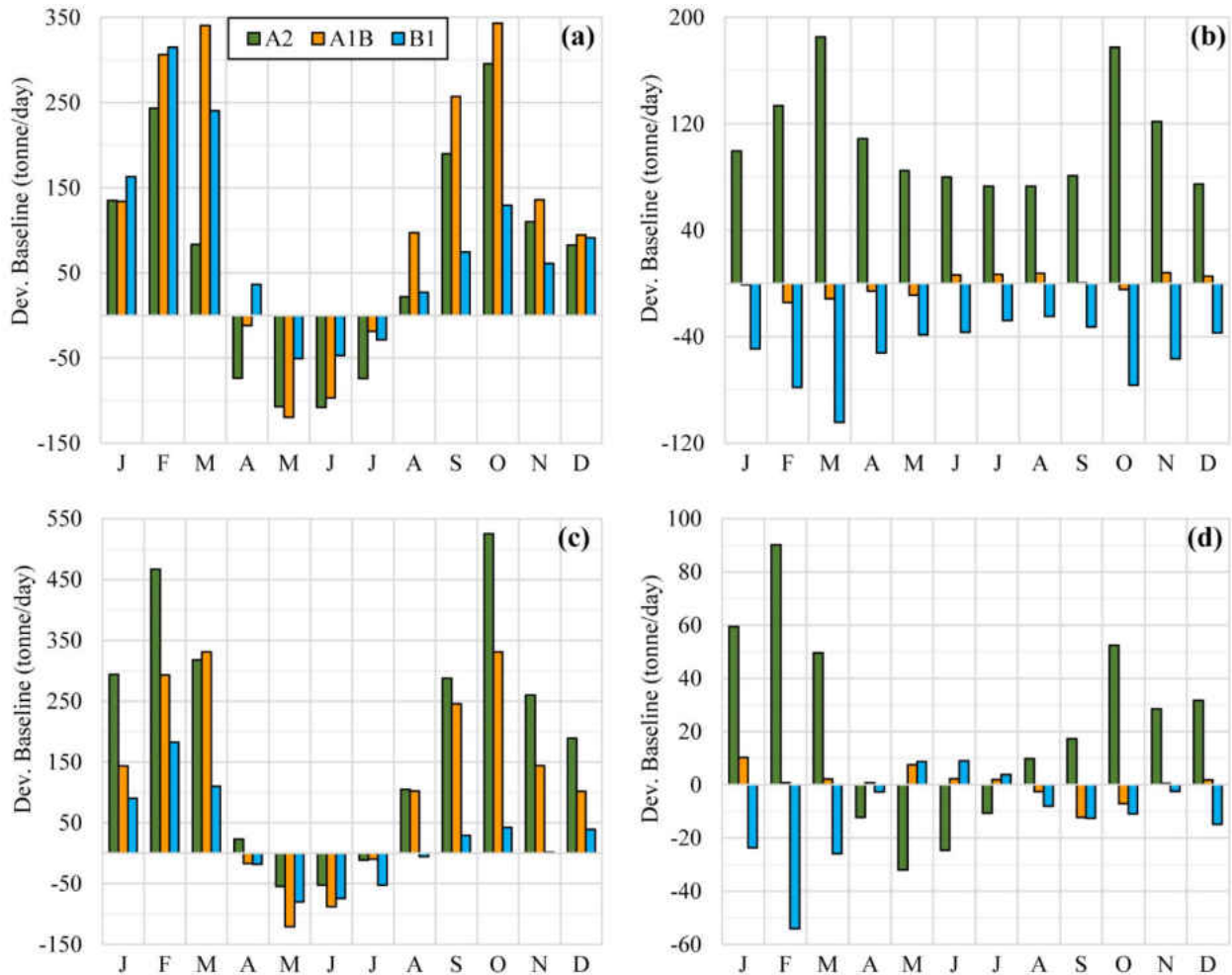
Figure 20 Future sediment loading deviations from the baseline for HADCM3 the A2 (green), A1B (orange) and B1 (blue) scenarios. (a) Climate only, (b) LULC only, (c) climate and LULC, and (d) deviations climate and LULC – (deviations climate only + deviations LULC only)

8.4.1 Seasonality

As seen with the climate only simulation, coupled climate and LULC change results show a large gradation in the results produced by different GCMs. The behaviors of runoff and sediment are very similar to the climate only simulation in regard to their increase or decreasing behaviors from the baseline. That is, the HADCM3 predicts higher high flows and lower low flows, IPCM4 indicates overall lowered streamflow, and MPEH5 produces generally increased flow. The general

83

seasonal behavior for sediment is also very similar. Including both climate and LULC caused a significant increase sediment loading for the A2 scenario, followed by the A1B, and lastly B1.

8.5 Model Response to Extreme Event

An analysis of the simulated response of streamflow and sediment loading was performed for an extreme event. The event was selected using the Weibull method to identify a 24 hour, 25 year return period for streamflow. Once the streamflow quantity having a 24hr-25yr return period was established for each simulation, a streamflow representative of the event and corresponding sediment loadings were extracted from each dataset.

The extreme event analyzes the both the peak and total quantities. Figure 21 shows the peak streamflow and sediment loading for the extreme events. The black bar indicates the present day peak streamflow and sediment at 5,353 cms and 58,420 tonnes/day, respectively. In the case of LULC only, the values only represent scenarios A2, A1B, and B1, not individual GCMs. The quantities shown in the graphs correspond with the scenarios labeling on the x-axis and are repeated for each GCM. Changes in LULC only, as indicated by the gold bars, did not change the peak discharge. Sediment loading was only mildly affected for A2, A1B, and B1, which were 58,460, 58400, and 58380 tonnes/day, respectively. The climate only simulation resulted in differing responses associated with the individual GCMs. Where HADCM3 and IPCM4 generally estimated a decrease in the peak discharge, MPEH5 predicted an increase. Despite the increase in streamflow for MPEH5, the sediment loading does not have a remarkable increase, and for A2 and A1B, the peak loading is actually expected to decrease. Additionally, the sediment load for IPCM4 is predicted to increase for A2, A1B, and B1 to 61,480, 61,820, 60,740 tonnes/day.   When

coupling both climate and LULC change, generally an increase in the peaks occurred compared to the climate only simulations however the trends between GCMs remained the same. The average percent increase / decrease of peak streamflow from the baseline when simulating climate and LULC change was -0.8%, -0.5% and 2.0% for HADCM3, IPCM4, and MPEH5, respectively. For sediment, the values changes by an average of -0.3%, 5.2%, and -0.1% for HADCM3, IPCM4, and MPEH5.
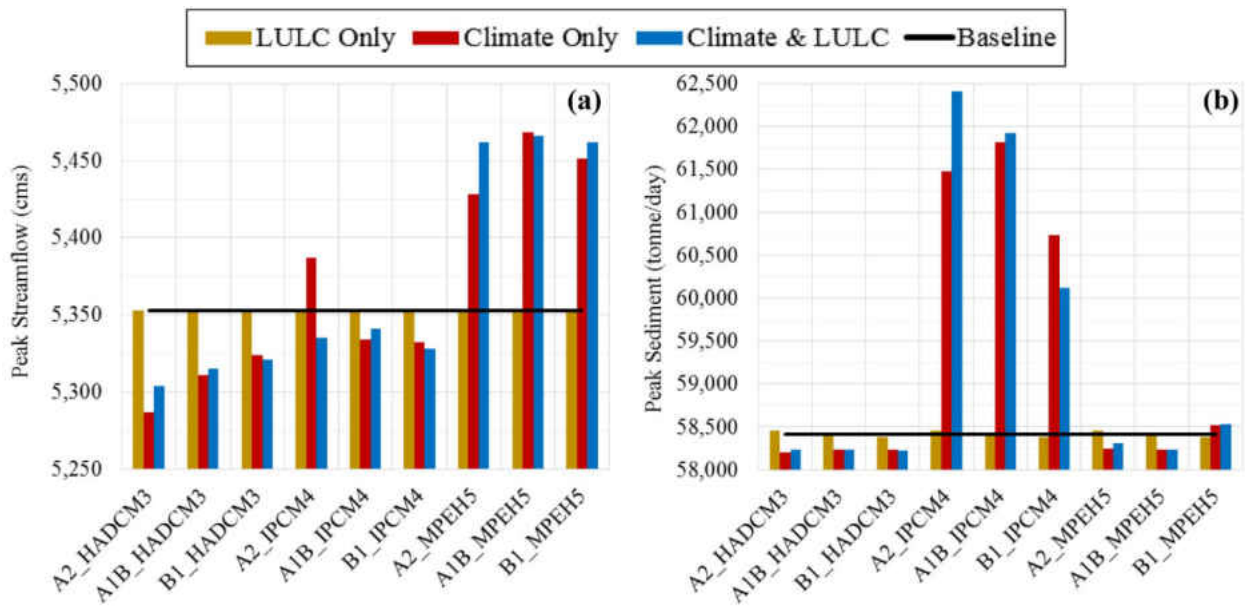
Figure 21 (a) Peak streamflow and (b) sediment loading for 24 hour, 25 year event

A 50 day period was extracted from each simulation dataset to incorporate the entirety of the event, including several days prior to the peak and the recession. The sums for both the streamflow and sediment loadings from all climate, LULC, and coupled climate and LULC simulations are shown in Figure 20. The baseline had a total discharge of 99,833 cms over the course of the event. The change in total streamflow resulting from LULC only change was minimal, as compared to the

baseline, with the A2, A1B, and B1 scenarios showing resulting in 100,217; 99,895; and 99,775 cms, respectively. In response to climate only, total streamflow showed a decrease for HADCM3 and IPCM4 whereas MPEH5 projected an increase. The MPEH5 percent increase from the baseline for A2, A1B, and B1 was a 5.4%, 3.8%, and 5.8%, respectively. The same patterns resulting from the climate only runs were displayed for the simulations that include climate and LULC change. The difference between the two simulation types was, for scenarios A2 and A1B total streamflow was increased by the coupling effect while a decrease occurred for B1, as predicted by all GCMs. Further, the increase from the baseline also responded in a nonlinear way. That is, for example, LULC only increased total streamflow from the baseline by 384 cms for A2, climate only increased by 5,429 cms for A2 MPEH5, and climate and LULC increased by 6,279 cms for A2 HADCM3.

Regarding the sediment loading, the baseline had a total amount of 640,649 tonnes/day over the 50 day period. Changes to LULC only caused sediment to increase for the scenarios A2 (644,832 tonnes/day) and A1B (641,173 tonnes/day) and to decrease for B1 (638,576 tonnes/day). The deviations from the baseline were more drastic for the sediment load however and for all GCMs, the A2 scenario produced the largest and B1 the smallest total sediment. Response to changes in climate only differed among the individual GCMs and scenarios. While HADCM3 and IPCM4 showed mixed increasing and decreasing, MPEH5 modeled an average increase from present conditions of 1.8%. For climate and LULC simulations, the response was similar to that of the streamflow, with total sediment load expected to be larger for A2 and A1B scenarios compared to the climate only simulations. The largest increase occurred for A2 MPEH5, which increased from the baseline by 3.2%. The largest decreased occurred for B1 IPCM4, which was a 0.4% decrease.

Where the increases or decreases in peak streamflow and sediment loading for the extreme event were not closely correlated, a more unified response was observed for the total amounts over the 50 day period. In general HADCM3 and IPCM4 predicted less streamflow for both the peak and totals where MPEH5 experienced larger values. Sediment loading had mixed responses for the peak from each GCM but in general over the entirely of the event, loading increased for all GCM for the A2 and A1B scenarios. The decreased sediment loading for the peak and increased loading over the 50 day period modeled by MPEH5 indicates a longer recession period.
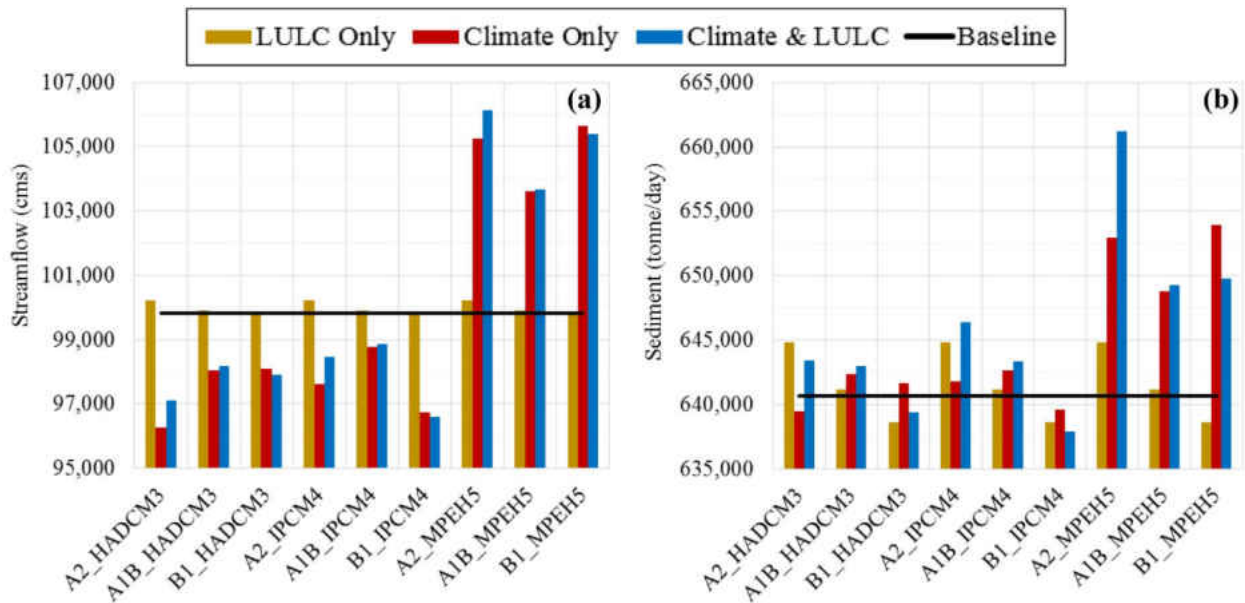

Figure 22 (a) Total streamflow (cms) and (b) total sediment loading (tonnes/day) over 50 day period incorporating 24 hour, 25 year return period event. The colors represent LULC only (gold), climate only (red), climate and LULC (blue) and the baseline (black).

CHAPTER 9: DISCUSSION

Climate change as predicted by the individual GCMs show noticeable differences in future rainfall seasonal patterns with no one carbon emission scenario resulting in higher values, emphasizing the structural differences among GCMs. The general consensus for temperature is that it will increase, with A2 predicting the highest values and B1 the lowest. When incorporating climate change into the SWAT model, output in terms of runoff and sediment loading showed large distinction between GCMs, implying that these parameters might be driven more by rainfall than temperature. Both the streamflow and sediment loading respond to future climate change, yet the ways in which they respond may be conflicting between GCMs. At present, high runoff occurs around October – December. All GCMs agree runoff will increase for the months of September and October, implying the current wet season may occur earlier in the year and with greater magnitude. In accompaniment, sediment loadings are also expected increase for these months. Further, loading for the baseline is at its minimum from July to September, yet a seasonal shift may occur with minimal loading happening earlier in the year, around April to June. This response may be driven by the lowered future precipitation that occurs within these months.

Incorporating the LULC change had little to no effect on the runoff response. Surface runoff is computed using the SCS curve number method, and the cumulative curve numbers for the c.2000, 2100 A2, A1B, and B1 land cover within the study domain are 46.9, 48.7, 45.7, and 44.4. The slight variability in curve number values might explain why streamflow is so minimally affected by LULC change. An alternative future LULC class assignment different than that produced in Table 7 could result in a more significant response. The slight increase that does occur from

August – October for the A2 land cover might be explained by the plant growth model that is incorporated into SWAT and associated evapotranspiration.

Sediment loading was far more impacted by changes made to land cover than runoff. The loading increase observed from the A2 LULC may be a result of the large increase in agricultural lands and loss of forested area. Sediment loading decreased for all month as a result of the B1 coverage. Compared to the c.2000 coverage, B1 has more forested regions and less agriculture. It is inferred that agricultural and forested lands are directly related to sediment loading and that an increase in agriculture and/or loss of forest may cause loading quantities to increase. The negative values associated with the IPCM4 model indicate more sediment is entering the river at the Jim Woodruff Dam than is exiting near the bay, suggesting sediment may settle prior to reaching the outlet. This may be caused by the decrease in rainfall and associated decline in runoff.

Runoff response for simulations that coupled climate and LULC change produced streamflow values that were very similar to those produced by incorporating climate change only, suggesting future climate change may affect flow more than LULC change. Coupling climate and LULC change caused future flow to deviate less from the baseline than combining results from isolated simulations, i.e. climate only and LULC only, indicating the interaction between projected changes to climate and land coverage may be more balanced in terms of runoff.

Sediment loading response was more reactive. Loadings for each GCM from largest to smallest was A2, A1B, and B1. Overall coupling of both climate and LULC change caused sediment load to be larger than adding isolated responses. When climate and LULC both independently modeled

sediment as increasing or as decreasing, the coupled response resulted in sediment values that were overall larger than would be estimated from the added, individual deviations from the baseline. This suggests climate and LULC change effects amplify one another, resulting in larger loadings than if estimated by the separately modeled responses. When individual response of climate only and LULC only differed in increase or decrease from the baseline, deviations swayed more in the direction of the climate induced shift, indicating climate may ultimately affect sediment more than land cover for this region.

CHAPTER 10: CONCLUSIONS AND FUTURE WORK

For this study, a hydrologic SWAT model was developed, calibrated and validated for the Apalachicola River Basin under historical conditions. Projected climate and LULC data were prepared to represent future conditions related to IPCC-SRES A2, A1B, and B1 for 2100. The datasets were assimilated into the model to assess the response of daily streamflow and sediment loading to changes in climate, LULC, and climate and LULC.

The findings from this research showed differing behaviors for both streamflow and sediment loading predicted by the global climate models. The variability in response to the GCMs further advocate the use of multi-model ensembles and additional research is needed to determine region specific performance of individual GCMs to better optimize model ensembles and eliminate erroneous outputs.

Despite contrasting outputs associated with the GCMs, all models indicate climate change may induce seasonal shifts that could extend or completely alter periods of high and low streamflow and sediment loading. Peak streamflow was predicted to occur earlier in the year, around September and October and minimum sediment loading also occurred earlier in the year, around April and June, as compared to present day conditions. Seasonal shifts in streamflow and sediment may affect the phenology of the ecosystem including dynamics related to migration, breeding, productivities, and distributions. Streamflow response to changes in LULC was minimal, however another classification scheme implemented other than that used for this study may result in a more significant reaction. Larger sediment loading was associated with increased agriculture, increased

urban areas, and decreased forested regions. As coastal regions become more urbanized, the increase in sediment may result in higher levels of total suspended solids that may affect oysters and seagrasses. A nonlinear response was observed when climate and LULC change were incorporated in the model simulation simultaneously, implying changes in one may exacerbate or dampen the effects of the other. The dynamic interaction that exists suggests both should be incorporated into hydrologic models when studying future conditions. Lastly, contrasting behaviors were observed for the peak and total quantity response of discharge and sediment load associated with a 24 hour, 25 year storm. Alterations to these components may result in changes to flooding and erosions rates, and future assessment of the downscaling approach to capture extreme events is needed.

The results from this study provide an improved understanding of the effects of climate and LULC change on water quantity and quality for the Apalachicola Bay and surrounding region as well as similar fluvial estuaries. The outcomes from this research can better guide management practices that may pertain to regulatory actions, land use development and planning, and monitoring activities. Outputs may be used in biological assessments as boundary conditions and inputs for models studying the ecology of this system, e.g., marshes, oysters, and seagrasses under present and future scenarios. The validated SWAT model can also be used in additional hydrologic studies that assess, but are not limited to, changes in climate and LULC. Future studies may address the assumptions held constant or omitted for this study including changes in human activities, e.g., future consumptive demand, dynamic response of habitats, e.g., marsh migration and freshwater-sea interaction, e.g., sea level rise impacts.

REFERENCES

Asselman, N. E. M., H. Middelkoop, and P. M. v. Dijk (2003), The impact of change in climate and land use on soil erosion, transport and deposition of suspended sediment in the River Rhine, *Hydrological Processes*, *17*(16), 3225-3244.

Binding, C. E., T. A. Greenberg, R. P. Bukata, D. E. Smith, and M. R. Twiss (2012), The MERIS MCI and its potential for satellite detection of winter diatom blooms on partialy ice-covered Lake Erie, *Journal of Plankton Research*, *0*(0), 1-5.

Cai, X., D. Wang, T. Zhu, and R. Claudia (2009), Assessing the regional variability of GCM simulations, *Geophysical Research Letters*, *36*(2).

Chaouch, N., M. Temimi, S. Hagen, J. Weishampel, S. Medeiros, and R. Khanbilvardi (2012), A synergetic use of satellite imagery from SAR and optical sensors to improve coastal flood mapping in the Gulf of Mexico, *Hydrological Processes*, *26*, 1617-1628.

Chen, J., X. Li, and M. Zhang (2005), Simulating the impacts of climate variation and land-cover changes on basin hydrology: A case study of the Suomo basin, *Science in China Earth Sciences*, *48*(9), 1501-1509.

Chen, X., K. Alizad, D. Wang, and S. C. Hagen (2014), Climate Change Impact on Runoff and Sediment Loads to the Apalachicola River at Seasonal and Event Scales, *Journal of Coastal Research*, *Special Issue*(68), 35-42.

Couch, C. A., E. H. Hopkins, and P. S. Hardy (1996), Influences of Environmental Settings on Aquatic Ecosystems in the Apalachicola-Chattahoochee-Flint River Basin*Rep. 95-4278*, US Geological Survey, Atlanta, Georgia.

Dekshenieks, M., E. E. Hofmann, J. M. Klinck, and E. N. Powell (2000), Quantifying the Effects of Environmental Change on an Oyster Population: A Modeling Study, *Estuaries*, *23*(5), 593-610.

Dutterer, A. C., C. Mesing, R. Cailteux, M. S. Allen, W. E. Pine, and P. A. Strickland (2012), Fish Recruitment is Influenced by River Flows and Floodplain Inundation at Apalachicola River, Florida, *River Research and Applications*.

Easterling, D. R., G. A. Meehl, C. Parmesan, S. A. Changnon, T. R. Karl, and L. O. Mearns (2000), Climate Extremes: Observations, Modeling, and Impacts, *Science*, *289*(5487), 2068-2074.

Elder, J. R., S. D. Flagg, and H. C. Mattraw, Jr. (1988), Hydrology and ecology of the Apalachicola River, Florida - a summary of the river quality assessment: U.S. Geological Survey Water-Supply Pater*Rep. 2196*, 46 pp.

ESA (2013), Space Debris, edited, European Space Agency.

Favis-Mortlock, D., and J. Boardman (1995), Nonlinear responses of soil erosion to climate change: a modelling study on the UK South Downs, *CATENA*, *25*(1-4), 365-387.

Foley, J. A., et al. (2005), Global Consequences of Land Use, *Science*, *309*(5734).

Fuelberg, H. E., and D. G. Bigger (1994), The Preconvective Environment of Summer Thunderstorms over the Florida Panhandle, *Weather and Forecasting*, *9*(3), 316-326.

Gassman, P. W., M. R. Reyes, C. H. Green, and J. G. Arnold (2007), The Soil and Water Assessment Tool: Historical Development, Applications, and Future Research Directions, *Transactions of the ASABE*, *50*(4), 1211-1250.

Gibson, C. A., J. L. Meyer, N. L. Poff, L. E. Hay, and A. Georgakakos (2005), Flow Regime Alterations under Changing Climate in Two River Basins: Implications for Freshwater Ecosystems, *River Research and Applications*, *21*(8), 849.

Gleick, P. H. (2003), Water Use, *Annnual Review of Environment and Resources*, *28*, 275-314.

Gupta, H., S. Sorooshian, and P. Yapo (1999), Status of Automatic Calibration for Hydrologic Models: Comparison with Multilevel Expert Calibration, *Journal of Hydrologic Engineering*, *4*(2), 135-143.

Hay, L. E., J. LaFontaine, and S. L. Markstrom (2014), Evaluation of Statistically Downscaled GCM Output as Input for Hydrological and Stream Temperature Simulation in the Apalachicola-Chattahoochee-Flint River Basin (1961-99), *Earth Interactions*, *18*(9).

Huang, W., and W. K. Jones (1997), Three-dimensional modeling of circulation and salinity for the low river flow season in Apalachicola Bay, FL*Rep.*, 120 pp.

IPCC (2000), Special Reports: Emissions Scenarios*Rep.*, IPCC, UK.

IPCC (2007), Climate Change 2007: The Physical Science Basis, *Rep.*, 966 pp, IPCC, Cambridge, United Kingdom and New York, NY, USA.

IPCC (2013), What is a GCM?, in *Guidance on the use of data*, edited, IPCC.

Isphording, W. C. (1986), Apalachicola Bay: Dynamic Sedimentation in a Gulf Coast Estuary, *Gulf Coast Association of Geological Societies Transactions*, *36*, 471-488.

Johnson, T. E., J. B. Butcher, A. Parker, and C. P. Weaver (2012), Investigating the Sensitivity of U.S. Streamflow and Water Quality to Climate Change: U.S. EPA Global Change Research Program's 20 Watersheds Project, *Journal of Water Resources Planning and Management*, *138*(5), 453-464.

Kaplan, J. O., K. M. Krumhardt, and N. Zimmermann (2009), The prehistoric and preindustrial deforestation of Europe, *Quaternary Science Reviews*, *28*(27-28), 3016-3034.

Karl, T. R., and R. W. Knight (1998), Secular Trends of Precipitation Amount, Frequency, and Intensity in the United States, *Bulletin American Meteorological Society*, *79*, 231-241.

Katz, R. W. (1996), Use of conditional stochastic models to generate climate change scenarios, *Climatic Change*, *32*(3), 237-255.

Klein Goldewijk, K. (2001), Estimating global land use change over the past 300 years: The HYDE Database, *Global Biogeochemical Cycles*, *15*(2), 417-433.

Krysanova, V., and R. Srinivasan (2015), Assessment of climate and land use change impacts with SWAT, *Regional Environmental Change*, *15*, 431-434.

Lambin, E. F., H. J. Geist, and E. Lepers (2003), Dynamics of Land-Use and Land-Cover Change in Tropical Regions, *Annnual Review of Environment and Resources*, *28*, 205-241.

Lambin, E. F., et al. (2001), The causes of land-use and land-cover change: moving beyond the myths, *Global Environmental Change*, *11*(4), 261-269.

Light, H. M., M. R. Darst, and J. W. Grubbs (1996), Aquatic Habitats in Relation to River Flow in the Apalachicola River Floodplain, Florida*Rep. Professional Paper 1594*, USGS, Washington.

Livingston, R. J. (1984), The ecology of the Apalachicola Bay system: an estuarine profile*Rep.*, 148 pp, U.S. Fish Wildlife Services.

Livingston, R. J., S. E. McGlynn, and X. Niu (1998), Factors controlling seagrass growth in gulf coastal system: Water and sediment quality and light, *Aquatic Botany*, *60*(2), 135-159.

Livingston, R. J., et al. (2000), Modelling Oyster Population Response to Variation in Freshwater Input, *Estuarine, Coastal, and Shelf Science*, *50*(5), 655-672.

Loveland, T. R., T. L. Sohl, S. V. Stehman, A. L. Gallant, K. L. Sayler, and D. E. Napton (2002), A Strategy for Estimating the Rates of Recent United State Land-Cover Changes, *Photogrammetic Engineering & Remote Sensing*, *68*(10), 1091-1099.

McNulty, J. K., W. N. Lindall, and J. E. Sykes (1972), Cooperative Gulf of Mexico estuarine invenory and study, Florida: phase 1, area description*Rep.*, 126 pp, U.S. Department of Commerce, National Oceanographic and Atmospheric Administration, and National Marine Fisheries Service, Seattle, Washington.

Mearns, L. O., F. Giorgi, P. Whetton, D. Pabon, M. Hulme, and M. Lal (2004), Guidelines for use of climate scenarios developed from regional climate model experiments*Rep.*, Data Distribution Centre of the Intergovernmental Panel on Climate Change.

Medeiros, S. C., T. Ali, S. C. Hagen, and J. P. Riaiford (2011), Development of a seamless topographic/bathymetric digital terrain model for Tampa Bay, Florida, *Photogrammetic Engineering & Remote Sensing*, *77*, 1249-1256.

Menne, M. J., I. Durre, R. S. Vose, B. E. Cleason, and T. G. Houston (2012), An Overview of the Global Historical Climatology Network-Daily Database, *Journal of Atmospheric and Oceanic Technology*, *29*, 897-910.

Milly, P. C. D., J. Betancourt, M. Falkenmark, R. M. Hirsch, Z. W. Kundzewicz, D. P. Lettenmaier, and R. J. Stouffer (2008), Stationarity Is Dead: Whither Water Management?, *Science*, *319*(5863), 573-574.

Moriasi, D. N., J. G. Arnold, M. W. V. Liew, R. L. Bingner, R. D. Harmel, and T. L. Veith (2007), Model Evaluation Guidelines for Systematic Quantification of Accuracy in Watershed Simulations, *Transactions of the ASABE*, *50*(3), 885-900.

Murphy, J. (1999), An Evaluation of Statistical and Dynamical Techniques for Downscaling Local Climate, *Journal of Climate*, *12*, 2256-2284.

Narsimlu, B., A. K. Gosain, and B. R. Chahar (2013), Assessment of Future Climate Change Impacts on Water Resources of Upper Sind River Basin, India Using SWAT Model, *Water Resources Management*, *27*(10), 3647-3662.

Nash, J. E., and J. V. Sutcliffe (1970), River flow forecasting through conceptual models part I - A discussion of principles, *Journal of Hydrology*, *10*(3), 282-290.

National Centers for Environmental Prediction (2015), Climate Forecast System Reanalysis, edited by T. A. M. A. Research, T. A. M. University, C. University, I. W. M. Institute, N. O. a. A. Administration and V. Tech.

Neitsch, S. L., J. G. Arnold, J. R. Kiniry, and J. R. Williams (2011), Soil and Water Assessment Tool Theoretical Documentation *Rep. 406*, USDA Agricultural Research Service (ARS) Grassland, Soil and Water Research Laboratory, Texas Agricultural Experiment Station, Blackland Research Center, Temple, TX.

Pal, I., B. T. Anderson, G. D. Salvucci, and D. J. Gianotti (2013), Shifting seasonality and increasing frequency of precipitation in we and dry seasons across the U.S., *Geophysical Research Letters*, *40*(15), 4030-4035.

Pan, S., G. Li, Q. Yang, Z. Ouyang, G. Lockaby, and H. Tian (2013), Monitoring Land-Use and Land-Cover Change in the Eastern Gulf Coastal Plain Using Multi-temporal Landsat Imagery, *Geophysics and Remote Sensing*, *2*(1).

Park, J.-Y., M.-J. Park, S.-R. Ahn, G.-A. Park, J.-E. Yi, G.-S. Kim, R. Srinivasan, and S.-J. Kim (2011), Assessment of Future Climate Change Impacts on Water Quantity and Quality for Mountainous Dam Watershed Using SWAT, *Transactions of the ASABE*, *54*(5), 1725-1737.

Phan, D. B., C. C. Wu, and S. C. Hsieh (2011), Impact of Climate Change on Stream Discharge and Sediment Yield in Northern Viet Nam, *Water Resources*, *38*(6), 827-836.

Pielke, R. A., Sr., G. Marland, R. A. Betts, T. N. Chase, J. L. Eastman, J. O. Niles, D. D. S. Niyogi, and S. W. Running (2002), The influence of land-use change and landscape dynamics on the climate system: relevance to climate-change policy beyon the radiative effect of greenhouse gases, *Phil. Trans. R. Soc. Lond. A*, 1705-1719.

Praskievicz, S., and H. Chang (2009), A review of hydrological modelling of basin-scale climate change and urban development impacts, *Progress in Physical Geography*, *33*(5), 650-671.

Richardson, C. W. (1981), Stochastic Simulation of Daily Precipitation, Temperature, and Solar Radiation, *Water Resources Research*, *17*(1), 182-190.

Scavia, D., et al. (2002), Climate change impacts on U.S. Coastal and Marine Ecosystems, *Estuaries*, *25*(2), 149-164.

Schilling, K. E., K.-S. Chan, H. Lui, and Y.-K. Zhang (2010), Quantifying the effect of land use land cover change on increasing discharge in the Upper Mississippi River, *Journal of Hydrology*, *387*(3-4), 343-345.

Schilling, K. E., M. K. Jha, Y.-K. Zhang, P. W. Gassman, and C. F. Wolter (2008a), Impact of land use and land cover change on the water balance of a large agricultural watershed: Historical effects and future directions, *Water Resources Research*, *44*(7), W00A09.

Schilling, K. E., M. K. Jha, Y.-K. Zhang, P. W. Gassman, and C. F. Wolter (2008b), Impact of land use and land cover change on the water balance of a large agricultural watershed: Historical effects and future directions, *Water Resources Research*, *44*(7).

SCS (1972), Section 4: Hydrology *In* National Engineering Handbook*Rep.*, Soil Conservation Service.

Semadeni-Davies, A., C. Hernebring, G. Svensson, and L.-G. Gustafsson (2008), The impacts of climate change and urbanisation on drainage in Helsingborg, Sweden: Suburban stormwater, *Journal of Hydrology*, *350*, 114-125.

Semenov, M. A., and E. M. Barrow (1997), Use of a stochastic weather generator in the development of climate change scenarios, *Climatic Change*, *35*, 397-414.

Semenov, M. A., and R. J. Brooks (1999), Spatial interpolatin of the LARS-WG stochasitc weather generator in Great Britain, *Climate Research*, *11*, 137-148.

Semenov, M. A., and P. Stratonovitch (2010), Use of multi-model ensembles from global climate models for assessment of climate change impacts, *Climate Research*, *41*, 1-14.

Shi, P.-J., Y. Yuan, J. Zheng, J.-A. Wang, Y. Ge, and G.-Y. Qiu (2007), The effect of land use/cover change on surface runoff in Shenzhen region, China, *CATENA*, *69*(1), 31-35.

Short, F. T. (1987), Effects of sediment nutrients on seagrasses: Literature review and mesocosm experiment, *Aquatic Botany*, *27*(1), 41-57.

Shrestha, B., M. S. Babel, S. Maskey, A. v. Griensven, S. Uhlenbrook, A. Green, and I. Akkharath (2013), Impact of climate change on sediment yield in the Mekong River basin: a case study of the Nam Ou basin, Lao PDR, *Hydrology and Earth System Sciences*, *17*, 1-20.

Small, C., and R. J. Nicholls (2003), A Global Analysis of Human Settle ment in Coastal Zones, *Journal of Coastal Research*, *19*(3), 584-599.

Sohl, T., and K. Sayler (2008), Using the FORE-SCE model to project land-cover change in the southeastern United States, *Ecological Modelling*, *219*, 49-65.

Sohl, T. L., K. L. Sayler, M. A. Drummond, and T. R. Loveland (2007), The FORE-SCE model: a practical approach for projecting land cover change using scenario-based modeling, *Journal of Land Use Science*, *2*(2), 103-126.

Srinivasan, R., and J. G. Arnold (1994), Integration of a Basin-Scale Water Quality Model with GIS, *Journal of the American Water Resources Association*, *30*(3), 453-462.

Taillant, J. D., and R. Picolotti (1999), The Uses of Satellite Imagery*Rep.*, Center for Human Rights and the Environment (CEDHA).

U.S. Geological Survey (2013), USGS NED 1/3 arc-second 2013 1 x 1 degreee ArcGRID, edited, U.S. Geological Survey, Reston, VA.

U.S.G.S. (2014), The Apalachicola-Chattahoochee-Flint (ACF) River National Water Quality Assessment (NAWQA) Program study, edited, U.S. Geological Survey.

United Nations, Department of Economic and Social Affairs, and Population Division (2015), World Population Prospects: The 2015 Revision*Rep.*, New York: United Nations.

US Department of Agriculture (USDA) (2007), Soil survey geographic database, edited by U. D. o. Agriculture, USDA, Washington, DC.

USGS (2001), National Water Information System in *(Water Data for the Nation)*, edited.

USGS (2012), Surface-Water Annual Statistics for Florida, edited.

USGS (2014a), National Assessment of Ecosystem Carbon Sequestration and Greenhouse Gas Fluxes, in *Spatially Explicit Modeling of Land Use and Land Cover*, edited, U.S. Geological Survey.

USGS (2014b), in *National Assessment of Ecosystem Carbon Sequestration and Greenhouse Gas Fluxes*, edited, US Geological Survey.

USGS EROS Center (2014), CONUS Modeled annual land-cover maps of the A1B, A2, and B1 scenario from 2006-2100, edited, U.S. Department of the Interior, U.S. Geological Survey.

Valdes, J. B., R. S. Seoane, and G. R. North (1994), A methodology for the evaluation of global warming impact on soil moisture and runoff, *Journal of Hydrology*, *161*(1-4), 389-413.

Veldkamp, A., and E. F. Lambin (2001), Predicting land-use change: editorial, *Agriculture, Ecosystems and Environment*, *85*(1-3), 1-6.

Vogelmann, J. E., S. M. Howard, L. Yang, C. R. Larson, B. K. Wylie, and J. N. V. Driel (2001), Completion of the 1990's National Land Cover Data Set for the conterminous United States, *Photogrammetric Engineering and Remote Sensing*, *67*, 650-662.

Wang, D., and M. Hejazi (2011), Quantifying the relative contribution of the climate and direct human impacts on mean annual streamflow in the contiguous United States, *Water Resources Research*, *47*.

Wang, D., S. C. Hagen, and K. Alizad (2013), Climate change impact and uncertainty analysis of extreme rainfall events in the Apalachicola River basin, Florida, *Journal of Hydrology*, *480*, 125-135.

Wang, H., W. Huang, M. A. Harwell, L. Edmiston, E. Johnson, P. Hsieh, K. Milla, J. Christensen, J. Stewart, and X. Lui (2008), Modeling oyster growth rate by coupling oyster population and hydrodynamic models for Apalachicola Bay, Florida, USA, *Ecological Modelling*, *211*(1-2), 77-89.

Wang, R., L. Kalin, W. Kuang, and H. Tian (2014), Individual and combined effects of land use/cover and climate change on Wolf Bay watershed streamflow in southern Alabama, *Hydrological Processes*, *28*, 5530-5546.

Ward, P. J., R. T. v. Balen, G. Verstraeten, H. Renssen, and J. Vandenberghe (2009), The impact of land use and climate change on late Holocene and future suspended sediment yield of the Meuse catchment, *Geomorphology*, *103*(3), 389-400.

Wilby, R. L. (1997), Non-stationarity in daily precipitation series: implication for GCM down-scaling using atmospheric circulation indices *International Journal of Climatology*, *17*, 439-454.

Wilby, R. L., S. P. Charles, E. Zorita, B. Timbal, P. Whetton, and L. O. Mearns (2004), Guidelines for Use of Climate Scenarios Developed from Statistical Downscaling Methods*Rep.*, Data Distribution Centre of the Intergovernmental Panel on Climate Change.

Wilks, D. S. (1992), Adapting Stochastic Weather Generation Algorithms for Climate Change Studies, *Climatic Change*, *22*(1), 67-84.

Williams, J. R. (1995), Chapter 25: The EPIC model, in *Computer Models of Watershed Hydrology*, edited by V. P. Singh, pp. 909-1000, Water Resources Publications.

Wischmeier, W. H., and D. D. Smith (1978), Predicting rainfall erosion losses: a guide to conservation planning, in *Agriculture Handbook 282*, edited, USDA-ARS.

Wischmeier, W. H., C. B. Johnson, and B. V. Cross (1971), A soil erodibility nomograph for farmland and construction sites, *Journal of Soil and Water Conservation*, *26*, 189-193.

Yan, B., N. F. Fang, P. C. Zhang, and Z. H. Shi (2013), Impacts of land use change on watershed streamflow and sediment yield: An assessment using hydrologic modelling and partial least squares regression, *Journal of Hydrology*, *484*, 26-37.

Zimmerman, J. B., J. R. Mihelcic, and J. Smith (2008), Global Stressors on Water Quality and Quantity, *Environmental Science and Technology*, *42*(12), 4247-4254.